Efficient Model-Order Reduction of Massively Coupled Multiport Interconnects using Waveform Relaxation

by

Mina Farhan

A thesis submitted to the Faculty of Graduate Studies and Research in partial fulfillment of the requirements for the degree of Master of Applied Sciences

Ottawa-Carleton Institute for Electrical and Computer Engineering

Department of Electronics

Faculty of Engineering

Carleton University

Ottawa, Ontario, Canada

September 2010

Your file Votre référence
ISBN: 978-0-494-71522-2
Our file Notre référence
ISBN: 978-0-494-71522-2

Abstract

Model order reduction (MOR) of massively coupled interconnects can significantly affect the simulation time in high speed designs. Recently, a new MOR method for massively coupled interconnects has been proposed. In this method, the multiport networks are decoupled into two port subnetworks using waveform relaxation and then each subnetwork is reduced independently. A detailed efficient implementation of this method is described in this thesis. In addition, a more robust time domain method for calculating the waveform relaxation sources is presented. A parallel implementation is also developed and the speedup characteristics of the parallel simulation are studied. Moreover, this new method has been extended to include transmission lines that are modeled using delay extraction-based passive compact transmission-line (DEPACT) macromodel.

Acknowledgments

I would like to express my gratitude to my co-supervisors, Prof. Michel Nakhla and Prof. Ram Achar, for their guidance, continuous encouragement, friendly motivation, patience and their valuable advise during my research journey. It would not have been possible without their help. One simply could not wish for a better or friendlier supervisors. I feel privileged to have them as my thesis supervisors.

I would like to give my especial thanks to my wife, Rimounda, for her loving support and encouragement. Her smile and love provided me with all the encouragement I needed to finish my thesis. I also thank her for her assistance in typing the thesis. Without her help it would not have been possible to finish typing on time.

I would also like to extend my gratitude to my parents, Adel and Sonia Farhan, and my brother, Michael, for their years of guidance and support. Thank you. I believe your patience finally paid off.

I also thank my colleague, Douglas Paul, for his valuable discussions. I really appreciate his help in C++. He helped me a lot in fixing and optimizing my code.

I also thank my colleague, Ashok Narayanan, for his friendly discussions. I also thank him for his comments on the earlier version of this thesis. He also helped me in coding some of the examples presented in my thesis.

Finally, I would like to acknowledge my colleagues in the CAD group, B.Nouri, N.Nakhla, D.Trifkovic, A.Saini, M.Siddique, Y.Hong, L.Filipovic. Their discussions, comments and ideas made my work an enjoyable experience. I also give my thanks to H.Dhindsa and A.Sridhar for their help and support during my thesis and for helping me settle down in Ottawa.

Contents

List of Figures

List of Tables

List of Symbols

t	Time.
z	Position along the transmission line.
d	The length of the transmission line.
s	Independent variable of the Laplace domain (compared with t in the time domain).
P	A selector matrix.
R, L, G, C	Matrices contain the p.u.l parameters of a multi-transmission lines.
Z_o	The characteristics impedance of coupled transmission lines.
m	The number of sections of the TL macromodel (Lumped segmentation or DEPACT).
$\boldsymbol{u}_{in}(t)$	Vector of the ports voltages in a multiport circuit.

$\boldsymbol{i}_{out}(t)$	Vector of the ports currents in a multiport circuit.
$\boldsymbol{C}_\phi$	A matrix describing the lumped memory elements of of the network ϕ.
$\boldsymbol{G}_\phi$	A matrix describing the lumped memoryless elements of the network ϕ.
$\boldsymbol{b}_\phi$	A selector matrix that maps the port voltages into the node space ϕ of the network.
$\boldsymbol{x}_\phi$	Vector of MNA system variables of the network ϕ.
$\boldsymbol{x}$	A vector containing the state space variables of a system.
$\boldsymbol{Q}$	A matrix whose columns form the orthogonal basis for the Krylov subspace.
$\boldsymbol{Y}$	The Y-parameters matrix of the system.
$\boldsymbol{I}$	Identity matrix.
$\eta_j(z,t)$,$\gamma_j(z,t)$	The WR sources for the distributed approach at position z and time t.
$i_{src,j}(z,t)$	The WR sources for the lossy section in the DEPACT macromodel.
N	The number of coupled transmission lines in an interconnect network.
N_ϕ	The number of the MNA variables of the network ϕ.

Abbreviations

KCL	Kirchhoff's Current Law
MNA	Modified Nodal Analysis – a technique for analyzing circuits
RLCG	Resistance-Inductance-Capacitance-Conductance – p.u.l parameter matrices of a transmission line
p.u.l	Per Unit Length
TL	Transmission Line
F.D.	Frequency Dependent Parameters
MoC	Method Of Characteristics
MRA	Matrix Rational Approximation
DEPACT	Delay Extraction-based Passive Compact Macromodeling Algorithm
WR	Waveform Relaxation

WR_TP	Waveform Relaxation based on Transverse partitioning
WR sources	Waveform Relaxation Sources
MOR	Model Order Reduction
AWE	Asymptotic Waveform Evaluation
PRIMA	Passive Reduced-order Interconnect Macromodeling Algorithm

Chapter 1

Introduction

1.1 Background and Motivation

Simulation of interconnect circuits plays an important role in signal integrity (SI) analysis of high speed circuits. If SI issues (e.g. crosstalk, attenuation ... etc.) are not accurately predicted during the design stage of high speed circuits, these issues can affect the system performance. One of the major problems in SI analysis is the simulation of high speed interconnects. This problem is mainly related to the fact that high speed interconnects are best represented in the frequency domain using telegrapher's equations [1], whereas non-linear devices, such as drivers and receivers, can only be represented in the time domain.

Several methods have been proposed to discretize the telegrapher's equations. The

main goal of these methods is to find time-domain macromodels that can be used to represent transmission line behavior during the transient simulation. One method, known as conventional lumped segmentation, uses cascaded RLC lumped sections [1] to represent the transmission line behavior. This method provides a straight forward solution to the mixed time/frequency problem during the simulation. However, a large number of lumped sections may be required to accurately represent the transmission line behavior. This large number of sections may result in very large circuit matrices that can significantly affect the simulation time.

Another method, known as Method of Characteristics (MOC), has been described in the literature [5, 6] for interconnect analysis. This method allows for a fast analysis of long low-loss lines. Moreover, the MOC ensures the causality of the resulting macromodel. One of the major disadvantages of the MOC is that it is difficult to model lossy interconnects. Another disadvantage is that using MOC does not guarantee the passivity of the resulting macromodel. If a stable but not passive circuit is connected to another passive circuit, the resulting system can be unstable [2].

Other methods have been successfully used to represent the transmission line in the time domain, such as matrix rational approximation (MRA) [7, 8] and delay extraction-based macromodeling (DEPACT) [9]. These methods are based on approximating the exponential stamp of the transmission line with a closed form function during transient simulation. Using the closed form function, a transmission line

macromodel can be easily derived in the form of ordinary differential equations that can be easily linked to nonlinear circuit simulators. However, if the interconnects structure contains massively coupled transmission lines, a large number of lumped components will be required to accurately capture the interconnect response. As a result, the computational cost of the transient simulation can be significantly high.

Model-order reduction methods have been proposed as an alternative to approximate the interconnects behavior using compact models. The goal of order reduction methods is to replace the large scale model of a system with a lower dimension model that has the same characteristics of the original system. Reduction methods can be broadly classified as, projection-based methods and SVD-based methods [10]. Projection-based methods, such as PRIMA [11], result in reduced models that match the first leading block moments of the original system. These methods are widely used due to their simplicity and efficient performance. However, the size of the reduced model is proportional to the number of ports. Therefore, these type of methods are limited to systems with small number of ports.

The SVD based methods use the concept of controllability and observability of the states of the original system to calculate the reduced model. These SVD methods have shown promising results in terms of efficiency and accuracy of the resulting model.

Due to the limitations of projection-based methods, these methods are not efficient

when applied to massively coupled interconnects that have large number of ports. To address this issue, a more efficient method was proposed in [12] for sparse reduction of massively coupled interconnects. In this method, waveform relaxation (WR) is used to improve the conventional MOR methods. Using WR, the multiport coupled transmission lines can be decoupled into two port subnetworks using waveform relaxation, and then each are reduced independently. It was shown that the computational cost of the new method only grows linearly with respect to the number of lines [12]. However, the main disadvantage when applying this method is that the relaxation sources are calculated in the frequency domain, which may affect the efficiency of this method.

The goal of the thesis is to present an efficient time domain approach for calculating the relaxation sources for the method proposed in [12]. A parallel implementation is also developed to show the speedup characteristics of this method when used on a multicore platform. Moreover, the method proposed in [12] is also extended to include transmission lines that are modeled using delay extraction-based passive compact transmission-line (DEPACT) macromodel.

1.2 Contributions

The main contributions of the thesis are:

1. In chapter 4, an efficient time domain approach based on the generalized Thevenin theorem for calculating the relaxation sources for the sparse and passive reduction method proposed in [12] is presented. The generalized Thevenin theorem for multiport circuits is used to avoid the transformation between frequency and time domains when calculating the waveform relaxation sources.

2. A parallel implementation is developed (chapter 4). The speedup and the CPU scalability of the parallel implementation are given. It is shown that the speedup increases significantly when the number of CPUs increases.

3. An efficient MOR method that can be used to simulate coupled transmission lines that are modeled using the DEPACT macromodel, is proposed (chapter 5). This MOR method is based on waveform relaxation [13] and model order reduction algorithm for RLC circuits with delay elements [14].

1.3 Organization of the Thesis

The thesis is organized as follows. Chapter (2) provides a review of transmission lines macromodeling techniques. Chapter (3) gives an overview for conventional MOR

algorithms. A detailed description of the MOR method that was proposed in [12] and details of the proposed time domain approach for calculating the relaxation sources are given in chapter (4). Various numerical examples that validate the accuracy and the efficiency of the new approach are also presented in chapter (4). A parallel implementation is also discussed. An efficient MOR algorithm for transmission lines that are modeled using DEPACT is introduced in chapter (5). Chapter (6) gives conclusions and proposed future research.

Chapter 2

Overview of Transmission Lines Macromodeling Techniques

High speed interconnects that are modeled as TLs are best described in the frequency domain and do not have a closed form representation in the time domain. However, there exists different types of models that can be used to represent high speed interconnects in the time-domain. These models are used to discretize the telegrapher's equations [1] that describe the behavior of the high speed interconnects. Using such models, the transmission line behavior can be linked to non-linear time-domain Spice like simulators.

This chapter reviews some of the models that are used for interconnects analysis. Section (2.1) provides an overview of telegrapher's equations that represent the

coupled multi-transmission lines. Section (2.2) describes the conventional lumped segmentation macromodel. Section (2.3) gives an overview of the method of characteristics (MoC). Section (2.4) provides an overview of the matrix rational approximation method, and section (2.5) presents a delay extraction-based passive compact transmission line macromodel.

2.1 Telegrapher's Equations

Consider the multiconductor transmission lines with N coupled conductors, shown in Fig. 2.1.

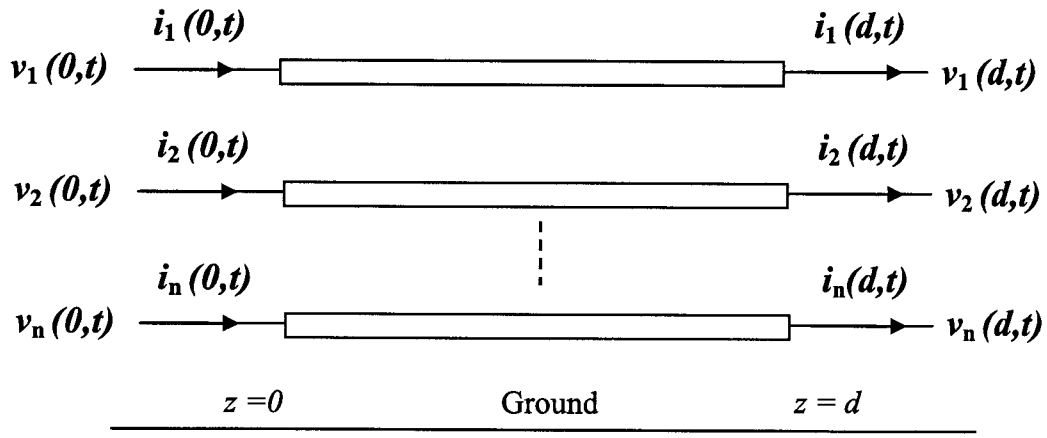

Figure 2.1: Multiconductor transmission lines

The telegrapher's equations [1] describing these multiconductor transmission lines

are given as

$$\begin{aligned} \frac{\partial}{\partial z}\boldsymbol{v}(z,t) &= -\boldsymbol{R}\boldsymbol{i}(z,t) - \boldsymbol{L}\frac{\partial}{\partial t}\boldsymbol{i}(z,t) \\ \frac{\partial}{\partial z}\boldsymbol{i}(z,t) &= -\boldsymbol{G}\boldsymbol{v}(z,t) - \boldsymbol{C}\frac{\partial}{\partial t}\boldsymbol{v}(z,t) \end{aligned} \tag{2.1}$$

where $\boldsymbol{R} \in \mathbb{R}^{N\times N}$, $\boldsymbol{L} \in \mathbb{R}^{N\times N}$, $\boldsymbol{C} \in \mathbb{R}^{N\times N}$ and $\boldsymbol{R} \in \mathbb{G}^{N\times N}$ are the per unit length (p.u.l) parameter matrices of the transmission lines , $\boldsymbol{v}(z,t) \in \mathbb{R}^N$ and $\boldsymbol{i}(z,t) \in \mathbb{R}^N$ are the voltage and current vectors of the transmission lines as a function of position z and time t.

The telegrapher's equations in (2.1) can be written in a matrix form as follows

$$\frac{\partial}{\partial x}\begin{bmatrix} \boldsymbol{v}(z,t) \\ \boldsymbol{i}(z,t) \end{bmatrix} = -\begin{bmatrix} \boldsymbol{0} & \boldsymbol{R} \\ \boldsymbol{G} & \boldsymbol{0} \end{bmatrix}\begin{bmatrix} \boldsymbol{v}(z,t) \\ \boldsymbol{i}(z,t) \end{bmatrix} - \begin{bmatrix} \boldsymbol{0} & \boldsymbol{L} \\ \boldsymbol{C} & \boldsymbol{0} \end{bmatrix}\frac{\partial}{\partial t}\begin{bmatrix} \boldsymbol{v}(z,t) \\ \boldsymbol{i}(z,t) \end{bmatrix} \tag{2.2}$$

The solution of the first order partial differential equations (PDE) given in (2.2) can be expressed in the frequency domain as [2]

$$\begin{bmatrix} \boldsymbol{V}(d,s) \\ \boldsymbol{I}(d,s) \end{bmatrix} = e^{(\boldsymbol{A}+s\boldsymbol{B})d}\begin{bmatrix} \boldsymbol{V}(0,s) \\ \boldsymbol{I}(0,s) \end{bmatrix} \tag{2.3}$$

where

$$\boldsymbol{A} = \begin{bmatrix} \boldsymbol{0} & -\boldsymbol{R} \\ -\boldsymbol{G} & \boldsymbol{0} \end{bmatrix}$$

$$\boldsymbol{B} = \begin{bmatrix} \mathbf{0} & -\boldsymbol{L} \\ -\boldsymbol{C} & \mathbf{0} \end{bmatrix}$$

$\boldsymbol{V}(d,s) \in \mathbb{R}^N$, $\boldsymbol{I}(d,s) \in \mathbb{R}^N$ are the Laplace transform of $\boldsymbol{v}(d,t)$ and $\boldsymbol{i}(d,t)$, respectively and d is the length of the transmission line.

It is to be noted that the exponential matrix $e^{(\boldsymbol{A}+s\boldsymbol{B})d}$ does not have a direct representation in time domain, whereas the nonlinear elements describing the terminations are represented in time domain. This problem is referred to in the literature as "Mixed time frequency" problem [2].

Several methods have been proposed to approximate (2.2) by a set of ordinary differential equations that can be linked to nonlinear circuit simulators. The following sections give an overview of some of these models, such as conventional lumped segmentation [1], the method of characteristics (MoC) [5, 6, 15], Matrix rational approximation (MRA) [7, 8, 16–18] and the delay extraction based passive compact transmission line macromodel (DEPACT) [3, 9, 19].

2.2 Conventional Uniform Lumped Segmentation Macromodel

In this macromodel, the coupled transmission lines behavior is represented by lumped RLC circuits that can be used in circuit simulators. If each line is divided into

m segments of length $\Delta z = \frac{d}{m}$, then the telegrapher's equations in (2.1) can be approximated by the following difference equations [1,2].

$$\frac{\boldsymbol{v}(z+\Delta z,t)-\boldsymbol{v}(z,t)}{\Delta z} = -\boldsymbol{R}\boldsymbol{i}(z,t)-\boldsymbol{L}\frac{\partial}{\partial t}\boldsymbol{i}(z,t) \quad (2.4)$$

$$\frac{\boldsymbol{i}(z+\Delta z,t)-\boldsymbol{i}(z,t)}{\Delta z} = -\boldsymbol{G}\boldsymbol{v}(z,t)-\boldsymbol{C}\frac{\partial}{\partial t}\boldsymbol{v}(z,t) \quad (2.5)$$

The equations in (2.4) and (2.5) can be represented using a cascade of lumped sections [1]. Fig. 2.2 shows two coupled transmission lines represented using conventional lumped segmentation, where $\hat{C}_{jj} = \sum_{k=1}^{2} C_{jk}$ and $\hat{G}_{jj} = \sum_{k=1}^{2} G_{jk}$ $(j = 1, 2)$ are the self capacitance and conductance of each line.

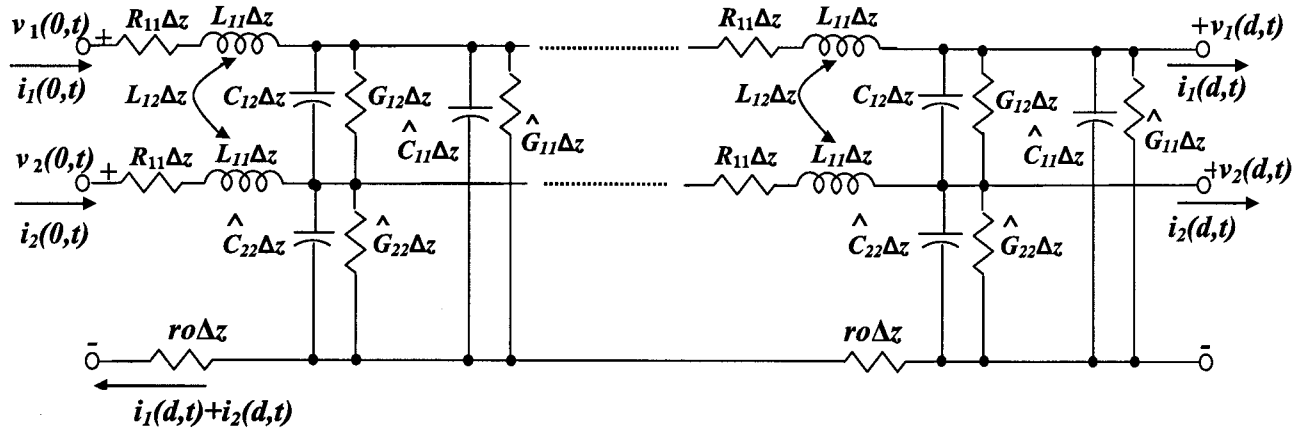

Figure 2.2: Uniform lumped segmentation model [1]

Approximating the telegrapher's equations using (2.4) and (2.5) is only valid if

the length of each segment is chosen to be smaller than the wavelength of interest (i.e. $\Delta z << \lambda$, where λ is the wavelength). As a practical guideline, the number of total lumped segments required to accurately represent a single transmission line behavior is given by [2]

$$m = \frac{10\tau d}{t_r}$$

where $\tau = d\sqrt{LC}$ is the per unit delay of the transmission line, t_r is the rise time of the propagating signal, L and C are the self inductance and capacitance of the line.

One of the major drawbacks of the conventional lumped segmentation model is that it requires very large number of sections, especially for circuits that are excited by sources with a sharp rise time [2]. This large number of sections leads to large circuit matrices, and hence the simulation of the transmission line becomes CPU intensive. In addition, the conventional lumped segmentation model cannot handle frequency dependent parameters (F.D.) [1].

2.3 Method of Characteristics (MoC)

As discussed earlier, in order to link the transmission line to time domain simulators, the partial differential equations of the transmission line in (2.3) should be transformed into ordinary differential equation. The MoC [5] was successfully used to do

such transformation for lossless transmission lines. Moreover, it can be extended to represent lossy transmission lines. Consider the telegrapher's equation for a single transmission line in the frequency domain

$$\frac{\partial}{\partial z}\boldsymbol{V}(z,s) = -R\boldsymbol{I}(z,s) - sL\boldsymbol{I}(z,s) \tag{2.6}$$

$$\frac{\partial}{\partial z}\boldsymbol{I}(z,s) = -G\boldsymbol{I}(z,s) - sC\boldsymbol{V}(z,s) \tag{2.7}$$

The equations in (2.6) and (2.7) can be represented in terms of Y-parameters [2,20] as

$$\begin{bmatrix} I(0,s) \\ I(d,s) \end{bmatrix} = \frac{1}{Z_o(1-e^{-2\gamma d})} \begin{bmatrix} 1+e^{-2\gamma d} & -2e^{-\gamma d} \\ -2e^{-\gamma d} & 1+e^{-2\gamma d} \end{bmatrix} \begin{bmatrix} V(0,s) \\ V(d,s) \end{bmatrix} \tag{2.8}$$

where γ and Z_o are the propagation constant and the characteristic impedance of the line, respectively, and they are defined as

$$\gamma = \sqrt{(R+sL)(G+sC)}$$

$$Z_o = \sqrt{\frac{R+sL}{G+sC}}$$

The terms in (2.8) can be re-arranged as follows [2]

$$V_0 = Z_o I_0 + e^{-\gamma d}[2V_d - e^{-\gamma d}(Z_o I_0 + V_0)] \tag{2.9}$$

$$V_d = Z_o I_d + e^{-\gamma d}[2V_0 - e^{-\gamma d}(Z_o I_d + V_d)] \tag{2.10}$$

(2.11)

where V_0, I_0, V_d and I_d represents the near and far-ends voltages and currents of the line, respectively

Next, (2.9) and (2.10) can be written as [2]

$$V_0 - Z_o I_0 = W_1 \tag{2.12}$$

$$V_d - Z_o I_d = W_2 \tag{2.13}$$

$$\tag{2.14}$$

where

$$W_1 = e^{-\gamma d}[2V_d - e^{-\gamma d}(Z_o I_0 + V_0)] \tag{2.15}$$

$$W_2 = e^{-\gamma d}[2V_0 - e^{-\gamma d}(Z_o I_d + V_d)] \tag{2.16}$$

Using (2.9)-(2.16), W_1 and W_2 can be expressed as

$$W_1 = e^{-\gamma d}[2V_d - W_2] \tag{2.17}$$

$$W_2 = e^{-\gamma d}[2V_0 - W_1] \tag{2.18}$$

If the transmission line is lossless, the propagation constant is purely imaginary, and is given by

$$\gamma = s\sqrt{LC}$$

Therefore, (2.17) and (2.18) can be written in time domain by replacing $e^{-\gamma d}$ with a time delay as [2]

$$w_1(t+\tau) = 2v_d(t) - w_2(t) \tag{2.19}$$

$$w_2(t+\tau) = 2v_0(t) - w_1(t) \tag{2.20}$$

$$\tag{2.21}$$

where

$$\tau = d\sqrt{LC}$$

Using the time domain expression in (2.19) and (2.20), the transmission line can be modeled using the characteristics impedance and two time delayed voltage controlled sources [2]. An equivalent circuit using MoC for a lossless transmission line is shown in Fig. 2.3. Since the MoC model is in time domain, it can be easily linked to time-domain simulators.

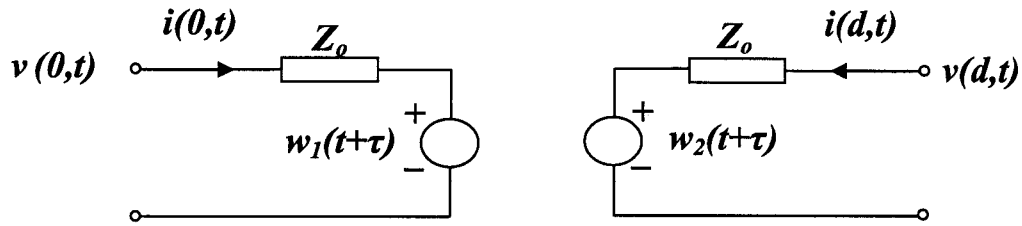

Figure 2.3: A lossless transmission line macromodel using MoC [2]

For lossy lines, the propagation constant (γ) is not purely imaginary and thus, it can not be replaced by a pure delay. To address this issue, the propagation constant

and the characteristic impedance (Z_o) can be represented as a rational function using Pade approximation [6] as follows

$$e^{-\gamma d} \approx e^{-s\tau} P(s) \tag{2.22}$$

where $P(s)$ is a rational function. Using (2.22), the MoC model can be extended for the case of N coupled transmission lines [6].

One of the major disadvantages of the MoC model is that the resulting models are not guaranteed to be passive. Stable but not passive models can lead to unstable systems when attached to arbitrary nonlinear elements. To address the passivity issue, MRA has been proposed in the literature [7,8,16]. Details of the MRA macromodel is given in the next section

2.4 Matrix Rational Approximation (MRA)

In MRA [7,8,16,18], the exponential matrix in (2.3) is approximated with a rational function using pre-determined coefficients. These coefficients can be calculated using closed form Pade' approximation. Since these coefficients are computed a priori, MRA does not suffer from the computationally expensive numerical algorithms associated with the MoC. In addition, the main advantage of MRA is that it is passive by construction.

Using Pade approximation, the exponential matrix in (2.3) can be expressed as

$$\boldsymbol{P}_{M_1,M_2}(\boldsymbol{Z})e^{\boldsymbol{Z}} = \boldsymbol{Q}_{M_1,M_2}(\boldsymbol{Z}) \tag{2.23}$$

$$\boldsymbol{Z} = (\boldsymbol{A} + s\boldsymbol{B})d \tag{2.24}$$

where $\boldsymbol{P}_{M_1,M_2}$ and $\boldsymbol{Q}_{M_1,M_2}(\boldsymbol{Z})$ are polynomial matrices expressed in terms of closed form Pade rational functions [7], as

$$\boldsymbol{P}_{M_1,M_2}(\boldsymbol{Z}) = \sum_{j=0}^{M_1} \frac{(M_1+M_2-j)!M_2!}{(M_1+M_2)!j!(M_1-j)!}(-\boldsymbol{Z})^j \tag{2.25}$$

$$\boldsymbol{Q}_{M_1,M_2}(\boldsymbol{Z}) = \sum_{j=0}^{M_1} \frac{(M_1+M_2-j)!M_2!}{(M_1+M_2)!j!(M_1-j)!}(\boldsymbol{Z})^j \tag{2.26}$$

The macromodel can be transformed to a set of ordinary differential equations using the co-efficients in (2.25) and (2.26). These differential equations can be easily linked to time-domain simulators as the stamp of the transmission line [17]. Moreover, it was proved in [8, 17] that using $M_1 = M_2$ in (2.25) and (2.26) will preserve the passivity of the macromodel.

The main disadvantage of the MRA macromodel is that there is no delay extraction before using the rational function approximation. In case of transmission lines with long delays MRA requires high order approximation to accurately capture the response of transmission lines. This high order approximation limits the usefulness of MRA to short lines with small delays.

2.5 Delay Extraction-Based Passive Compact Macromodeling (DEPACT)

DEPACT macromodel has been proposed in the literature [3,9,19] to address the issue of higher order approximation in MRA, especially in case of long delays lines. In this macromodel, the exponential matrix in (2.3) is approximated in terms of product of exponential matrices using Lie product formula [21]. The DEPACT macromodeling preserves the passivity of the macromodel. Moreover, the number of sections required to accurately represent the transmission line is small compared to the lumped segmentation and MRA macromodeling [3].

Consider the exponential matrix stamp of the transmission line

$$\begin{bmatrix} \boldsymbol{V}(d,s) \\ \boldsymbol{I}(d,s) \end{bmatrix} = e^{(\boldsymbol{A}+s\boldsymbol{B})d} \begin{bmatrix} \boldsymbol{V}(0,s) \\ \boldsymbol{I}(0,s) \end{bmatrix} \tag{2.27}$$

In case of lines with long delays, the modified Lie product formula can be used to approximate the exponential stamp of the transmission line [3,21]. The exponential matrix $e^{(\boldsymbol{A}+s\boldsymbol{B})d}$ can be expressed as

$$e^{(\boldsymbol{A}+s\boldsymbol{B})d} = \prod_{k=1}^{m} e^{s\boldsymbol{B}\frac{d}{2m}} e^{\boldsymbol{A}\frac{d}{m}} e^{s\boldsymbol{B}\frac{d}{2m}} + \epsilon_m \tag{2.28}$$

where the error $||\epsilon_m|| \equiv O(\frac{1}{m^2})$ and m is the order of the approximation. Using (2.28), the transmission line can be represented as a cascade of m lossless and lossy sections.

In case of multi-transmission lines with frequency independent parameters, the lossless section represented by $e^{s\boldsymbol{B}\frac{d}{2m}}$ can be realized using MOC macromodel, while the lossy section can be realized as a resistive network [3].

Consider the exponential stamp of the lossy section

$$\begin{bmatrix} \boldsymbol{V}_2 \\ \boldsymbol{I}_2 \end{bmatrix} = e^{\boldsymbol{A}\frac{d}{m}} \begin{bmatrix} \boldsymbol{V}_1 \\ \boldsymbol{I}_1 \end{bmatrix} \tag{2.29}$$

where $\boldsymbol{V}_1$, $\boldsymbol{I}_1$, $\boldsymbol{V}_2$ and $\boldsymbol{I}_2$ are the voltage and current vectors of the near and far-ends of the lossy sections, respectively. (2.29) can be written in terms of y-parameters as

$$\begin{bmatrix} \boldsymbol{I}_1 \\ \boldsymbol{I}_2 \end{bmatrix} = \boldsymbol{Y} \begin{bmatrix} \boldsymbol{V}_1 \\ \boldsymbol{V}_2 \end{bmatrix} \tag{2.30}$$

The y-parameters in (2.30) can be realized with a resistive network [3], as follows. The diagonal elements (Y_{jj}, $1 < j < N$) represent a resistor ($r_{jj} = \frac{1}{\sum_{k=1}^{2N} Y_{jk}}$) between node j and the ground, and the off-diagonal elements (Y_{jk}, $1 < j < N$, $1 < k < N$) represent a resistance ($r_{jk} = \frac{-1}{Y_{jk}}$) between node j and k. It worth noting that the off-diagonal elements (y_{jk}) are negative. Therefore, all resistors values are positive [3]. Fig. 2.4 shows the m^{th} DEPACT cell of a single transmission line, where $\boldsymbol{C}_m = \frac{\boldsymbol{C}}{2m}d$, $\boldsymbol{L}_m = \frac{\boldsymbol{L}}{2m}d$, $\boldsymbol{R}_m = \frac{\boldsymbol{R}}{m}d$ and $\boldsymbol{G}_m = \frac{\boldsymbol{L}}{m}d$

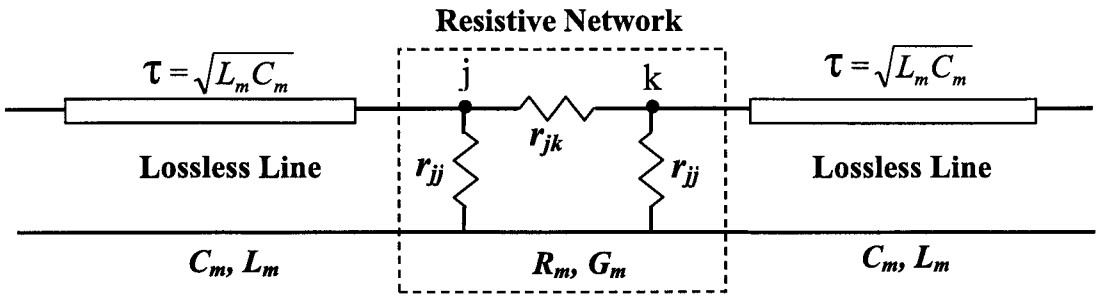

Figure 2.4: Depact section for a single transmission line [3]

2.6 Summary

In this chapter, an overview of the relevant macromodeling techniques for high-speed interconnects has been discussed. Conventional lumped segmentation, the method of characteristics (MoC), matrix rational approximation (MRA) and delay based extraction (DEPACT) were presented. The merits and demerits of each macromodel have been highlighted.

Chapter 3

Review of Model-Order Reduction (MOR)

As was discussed in the previous chapters, the approximation of a transmission line using lumped sections is only valid if the length of each section (Δx) is small compared to the wavelength ($\Delta x \leq \lambda$). If the line is electrically long ($d > 0.1\lambda$), a large number of lumped sections will be required to accurately model the electrical behavior of the transmission line. This large number of sections may lead to very large circuit matrices that would be inefficient to simulate.

The computational effort needed to perform the time domain simulation on a long lumped model has prompted research efforts to focus on MOR algorithms that can be used to extract a reduced macromodel. An important class of MOR techniques is

based on moment matching techniques [22] [23] [11]. In these MOR techniques, the original system transfer function and the macromodel transfer function share the first few leading moments.

The rest of the chapter is organized as follows. Section (3.1) describes the problem formulation. Section (3.2) gives an overview of explicit moment matching macromodeling algorithms using Asymptotic Waveform Evaluation (AWE). Section (3.3) presents implicit moment matching MOR algorithms based on Krylov subspace projection methods and section (3.4) presents a reduction algorithm for networks with delay elements.

3.1 Problem Formulation

Consider the time domain MNA description of a p-ports linear circuit that is given by [24, 25]

$$\boldsymbol{G}_\phi \boldsymbol{x}_\phi(t) + \boldsymbol{C}_\phi \dot{\boldsymbol{x}}_\phi(t) = \boldsymbol{b}_\phi \boldsymbol{w}_{in}(t) \tag{3.1}$$

$$\boldsymbol{w}_{out}(t) = \boldsymbol{L}^T \boldsymbol{x}_\phi(t) \tag{3.2}$$

where

- $\boldsymbol{G}_\phi$ and $\boldsymbol{C}_\phi \in \mathbb{R}^{N_\phi \times N_\phi}$ are constant matrices describing lumped memoryless and memory elements of the network, respectively,

- $\boldsymbol{x}_\phi \in \mathbb{R}^{N_\phi}$ is the vector of node voltage waveforms appended by waveforms of independent voltage source currents and inductor currents,
- $\boldsymbol{b}_\phi \in \mathbb{R}^{N_\phi \times p}$ is a selector matrix that maps the port voltages into the node space ϕ of the network,
- $\boldsymbol{w}_{in}(t) \in \mathbb{R}^p$, $\boldsymbol{w}_{out}(t) \in \mathbb{R}^p$ are the vectors of input excitations and the output variables at the ports of the linear circuit, respectively,
- N_ϕ is the number of MNA variables,
- the superscript T denotes the transpose.

In this chapter, the Y-parameters matrix will be used to represent the multiport circuit due to the relative simplicity of inserting the reduced Y-parameters matrix in the MNA equations of the complete circuit. In the case of the Y-parameters formulation of the circuit, voltage sources should be connected to the terminal ports of the circuit and the currents flowing into these ports should be considered as the output. In this case, it can be shown that

$$\boldsymbol{G}_\phi \boldsymbol{x}_\phi(t) + \boldsymbol{C}_\phi \dot{\boldsymbol{x}}_\phi(t) = \boldsymbol{b}_\phi \boldsymbol{u}_{in}(t) \tag{3.3}$$

$$\boldsymbol{i}_{out}(t) = \boldsymbol{b}_\phi^T \boldsymbol{x}_\phi(t) \tag{3.4}$$

where $\boldsymbol{u}_{in}(t)$, $\boldsymbol{i}_{out}(t)$ are vectors that contain the voltages and currents waveforms at the ports of the multiport circuit, respectively. The admittance matrix of the system

represented by (3.3) and (3.4) is given by [24]

$$\boldsymbol{Y}(s) = \boldsymbol{b}_{\phi}^{T}(\boldsymbol{G}_{\phi} + s\boldsymbol{C}_{\phi})^{-1}\boldsymbol{b}_{\phi} \tag{3.5}$$

The Y-parameters matrix obtained using (3.5) can be inserted into the MNA equations of a general nonlinear circuit as described in [2]. In the case of large circuits, the order of Y-parameters matrix becomes significantly large. Therefore, simulating the full circuit with nonlinear terminations becomes inefficient.

In the next sections, various model order reduction techniques will be presented. These techniques are used to approximate the Y-parameters matrix in (3.5), with a lower order matrix during the simulation of the circuit. It worth noting that, model order reduction techniques can be applied to other parameters such as Z-parameters. In this case, the input and output variables (w_{in} and w_{out}) of MNA equations in (3.1) and (3.2) will change slightly to reflect the required variables.

3.2 Model-Order Reduction based on AWE

The AWE [22] [26] moments matching technique is based on Pade' rational approximation. Consider the admittance matrix $\boldsymbol{Y}(s)$ of a multiport circuit. This admittance matrix $\boldsymbol{Y}(s)$ can be approximated by a rational function as

$$Y_{ij}(s) \approx \hat{Y}_{ij}(s) = \frac{\sum_{p=0}^{L} a_{p,ij}s^{p}}{1 + \sum_{q=1}^{M} b_{q,ij}s^{q}} = \frac{P_{L,ij}(s)}{Q_{M,ij}(s)} \tag{3.6}$$

where $\hat{Y}_{ij}$ is the component of the reduced Y-parameters matrix $\hat{\boldsymbol{Y}}(s)$ at the i^{th} row and j^{th} column, $a_{p,ij}$, $b_{q,ij}$ are the coefficients of the polynomials $P_{L,ij}(s)$ and $Q_{m,ij}(s)$, respectively.

Each component of the reduced admittance matrix $\hat{\boldsymbol{Y}}(s)$ can be represented using the Taylor series expansion at $(s = 0)$, in terms of its moments, as

$$\hat{Y}_{ij}(s) \approx \frac{\sum_{p=0}^{L} a_{p,ij} s^p}{1 + \sum_{q=1}^{M} b_{q,ij} s^q} \approx \sum_{k=0}^{(L+M)} m_{k,ij} s^k \tag{3.7}$$

where $m_{k,ij}$ are the moments of the admittance function $\hat{Y}_{ij}(s)$.

To evaluate the moments of the Y-parameters matrix in (3.7), we need to calculate the moments of the circuit. It can be shown that the moments of the entire multiport circuit can be calculated recursively as [2, 22]

$$\boldsymbol{G_\phi M_0} = \boldsymbol{b_\phi} \tag{3.8}$$

$$\boldsymbol{G_\phi M_k} = -\boldsymbol{C_\phi M_{k-1}} \tag{3.9}$$

The moments of the particular output of interest (In this case, the outputs are chosen to be the ports currents) are picked from moments matrix $\boldsymbol{M_k}$. Using (3.8) and (3.9), the coefficient of the polynomials $P_{L,ij}(s)$ and $Q_{M.ij}(s)$ of the required component of the admittance matrix can be calculated using the following formula [2]

$$\begin{bmatrix} m_{L-M+1} & m_{L-M+2} & \cdots & m_{L} \\ m_{L-M+2} & m_{L-M+3} & \cdots & m_{L+1} \\ \vdots & \vdots & \vdots & \vdots \\ m_{L} & m_{L+1} & \cdots & m_{L+M-1} \end{bmatrix}_{ij} \begin{bmatrix} b_M \\ b_{M-1} \\ \vdots \\ b_1 \end{bmatrix}_{ij} = - \begin{bmatrix} m_{L+1} \\ m_{L+2} \\ \vdots \\ m_{L+M} \end{bmatrix}_{ij} \tag{3.10}$$

The numerator coefficients can be calculated as [2]

$$a_{k,ij} = m_{k,ij} + \sum_{p=1}^{min(k,M)} b_{p,ij} m_{(k-p),ij} \tag{3.11}$$

Moreover, a pole-residue model can be found using the previously computed coefficient (i.e. $a_{k,ij}$ and $b_{k,ij}$). The poles ($P_{q,ij}$, $0 \leq q \leq M-1$) are obtained by finding the roots of the denominator polynomial $Q_{M,ij}(s)$. The residues ($K_{q,ij}$, $0 < q < L+M$) can be calculated by expanding the reduced admittance function $\hat{Y}_{ij}(s)$ using Taylor series and equating the coefficients of similar powers of s, more details can be found in [2].

The resulting reduced pole residue model can be inserted in the MNA of the main circuit with non-linear components. More details about inserting the reduced model in the main circuit can be found in [2,24].

One of the major drawbacks of the AWE is that it suffers from numerical illconditioing when used for higher order approximations. This is mainly related to the explicit moment matching technique used in the algorithm. It can be shown that the moments converge to the eigen vector corresponding to the Eigen value with largest

magnitude of the matrix $\boldsymbol{G}^{-1}\boldsymbol{C}$ [2]. Thus, increasing the number of moments will not yield any improvements of the results [27] [28].

3.3 Model-Order Reduction based on Projection Methods

In this section, we review another class of MOR techniques that are based on projection methods on the Krylov subspace to obtain a reduced model. These techniques provide a robust method for matching the leading moments of the system. Moreover, they do not suffer from the numerical limitations as in AWE.

First we will start by explaining the Krylov subspace, then we will discuss two methods used for extracting the reduced model using the orthonormal bases of the Krylov subspace.

Consider the MNA equations of multiport linear circuit given in (3.3) and (3.4). We define the two matrices, $\boldsymbol{A}_\phi = -\boldsymbol{G}_\phi^{-1}\boldsymbol{C}_\phi$ and $\boldsymbol{R}_\phi = \boldsymbol{G}_\phi^{-1}\boldsymbol{b}_\phi$. The MNA of the multiport circuit can be written as [2]

$$\boldsymbol{A}_\phi \dot{\boldsymbol{x}}_\phi(t) = \boldsymbol{x}_\phi(t) - \boldsymbol{R}_\phi \boldsymbol{u}_{in}(t) \tag{3.12}$$

$$\boldsymbol{i}_{out}(t) = \boldsymbol{b}_\phi^T \boldsymbol{x}_\phi(t) \tag{3.13}$$

Taking the Laplace transformation of (3.12) and (3.13) and with some mathematical manipulations, it can be shown that the block moments of the admittance matrix

are given by $\boldsymbol{b}_\phi^T \boldsymbol{A}_\phi^i \boldsymbol{R}_\phi$, $i = 0, \ldots, q$, where q is the number of terms (moments) that gives a good approximation of the admittance matrix $\boldsymbol{Y}(s)$ [2].

Next, we define Krylov subspace, which spans k columns, to be [11]

$$Kr(\boldsymbol{A}_\phi, \boldsymbol{R}_\phi, k) = span\{\boldsymbol{R}_\phi, \boldsymbol{A}_\phi \boldsymbol{R}_\phi, \ldots, \boldsymbol{A}_\phi^{q-1} \boldsymbol{R}_\phi\} \tag{3.14}$$

where $q = \lfloor \frac{k}{p} \rfloor$, p is the number of ports and $\lfloor * \rfloor$ represents the nearest integer operator, toward zero.

The Krylov subspace defined in (3.14) can be used to find an approximate solution of the circuit MNA equations in (3.3) and (3.4). The next sections discuss two methods that use projection onto the Krylov subspace to find the reduced model of the multiport network.

3.3.1 Block Arnoldi

The Block Arnoldi method [29] is used to generate orthonormal basis for the Krylov subspace through a recursive process.

Consider the matrix $\boldsymbol{Q}$ whose columns form the orthonormal bases for the Krylov subspace given in (3.14).

$$\boldsymbol{Q} = [v_1 \; v_2 \; \ldots \; v_k] \tag{3.15}$$

where v_i, $i = 1, ..., k$, is the i^{th} column of the matrix $\boldsymbol{Q}$, and $||v_i|| = 1$. The matrix $\boldsymbol{Q}$ can be calculated recursively using the block Arnoldi algorithm. Algorithm 3.3.1

presents the pseudo-code for the steps used in generating the orthonormal matrix $\boldsymbol{Q}$ using the the block Arnoldi algorithm [24].

Algorithm 1 Generate orthonormal bases of the Krylov subspace

1: Find QR factorization $\boldsymbol{R} = \boldsymbol{Q}_0\boldsymbol{V}$
2: **for** $j = 1$ to k **do**
3: Solve for $\boldsymbol{z}$ in $\boldsymbol{G}\boldsymbol{z} = \boldsymbol{C}\boldsymbol{Q}_j$
4: **for** $i = 1$ to j **do**
5: set $\boldsymbol{H}_{ij} = \boldsymbol{Q}_i^T\boldsymbol{z}$
6: set $\boldsymbol{z} = \boldsymbol{z} - \boldsymbol{H}_{ij}\boldsymbol{Q}_i$
7: **end for**
8: Find QR factorization $\boldsymbol{z} = \boldsymbol{Q}_j\boldsymbol{H}_{j(j-1)}$
9: **end for**
10: set $\boldsymbol{Q} = [\boldsymbol{Q}_0\ \boldsymbol{Q}_1 \ldots]$

Using the matrix $\boldsymbol{Q}$, the reduced model can be found by applying the orthogonal projection on the original multiport circuit, as follows [24]

$$\boldsymbol{x}_\phi = \boldsymbol{Q}\hat{\boldsymbol{x}} \tag{3.16}$$

Substituting (3.16) in (3.12), the reduced order model becomes

$$\hat{\boldsymbol{A}}\dot{\hat{\boldsymbol{x}}} = \hat{\boldsymbol{x}} - \hat{\boldsymbol{R}}u_{in}(t) \tag{3.17}$$

$$\boldsymbol{i}_{out}(t) = \boldsymbol{b}_\phi^T\hat{\boldsymbol{x}}_\phi(t) \tag{3.18}$$

where $\hat{\boldsymbol{A}} = \boldsymbol{Q}^T \boldsymbol{A}_\phi \boldsymbol{Q}$, $\hat{\boldsymbol{R}} = \boldsymbol{Q}^T \boldsymbol{R}_\phi$ and the admittance matrix can be represented as

$$\hat{\boldsymbol{Y}}(s) = \hat{\boldsymbol{b}}_\phi^T (\boldsymbol{I} - s\hat{\boldsymbol{A}})^{-1} \hat{\boldsymbol{R}} \tag{3.19}$$

It can be shown that the reduced macromodel, using Arnoldi algorithm, matches the first q block moments of the original system [11] [29].

The block Arnoldi algorithm does not suffer from numerical limitations compared to AWE. However, the block Arnoldi algorithm does not guarantee the passivity of the reduced model. This disadvantage limits the usage of the algorithm, because if a stable but not passive system is connected to other passive systems, it may lead to unstable system [2].

3.3.2 Passive Reduced-order Interconnect Macromodeling Algorithm (PRIMA)

This method is based on the Krylov subspace projection method, similar to the block Arnoldi method discussed in the previous section. However, PRIMA [11] uses double matrix projection for $\boldsymbol{G}_\phi$ and $\boldsymbol{C}_\phi$, which is different than the block Arnoldi method that uses single matrix projection for $\boldsymbol{A}_\phi$. Moreover, PRIMA guarantees that the reduced model is stable and passive.

Consider the MNA equations of multiport linear circuit given in (3.3) and (3.4). To preserve the passivity of the reduced macromodel, the following modifications in

the MNA formulation are required [11]

$$C_\phi = \begin{bmatrix} C_a & 0 \\ 0 & C_b \end{bmatrix} \quad G_\phi = \begin{bmatrix} G_a & P \\ -P^T & 0 \end{bmatrix} \tag{3.20}$$

where G_a, C_a and C_b are matrices that contain the stamps of the resistor, capacitor and inductors, respectively. Matrix P is a selector matrix contains only {1,-1,0} that represents the current variables in the MNA equations.

From (3.20), it can be proven that C_a, C_b and G_a are symmetric positive semi-definite matrices. Therefore using the MNA formulation in(3.20) results in a symmetric positive semi-definite G_ϕ and C_ϕ [11,24].

Using the MNA formulation in (3.20), the orthonormal matrix Q can be evaluated using the block Arnoldi algorithm discussed earlier in section 3.3.1. The reduced order system can then be obtained using congruence transformation as follows [11]

$$\hat{G}_\phi \hat{x}(t) + \hat{C}_\phi \dot{\hat{x}}(t) = \hat{b}_\phi u_{in}(t) \tag{3.21}$$

$$i_{out}(t) = \hat{b}_\phi^T \hat{x}(t) \tag{3.22}$$

where

$$\hat{G}_\phi = Q^T G_\phi Q \tag{3.23}$$

$$\hat{C}_\phi = Q^T C_\phi Q \tag{3.24}$$

$$\hat{b}_\phi = Q^T b_\phi \tag{3.25}$$

$$\tag{3.26}$$

The major disadvantage of Krylov subspace projection methods is that the size of the reduced model depends on the number of ports of the multiport circuit. In the case of massively coupled multiport interconnects circuits, the size of the reduced model increases significantly. This disadvantage limits the usage of these methods to interconnect circuits with relatively small number of transmission lines.

3.4 Model-Order Reduction for RLC Circuits with Delay Elements

Model order reduction techniques, based on the Krylov subspace, can only be applied to passive RLC circuits. In the case of circuits with delay elements, MOR algorithms based on moment matching can not be directly applied to such circuits.

In [14], a MOR algorithm has been suggested for networks with delay elements. Delay elements can exist in a network if a delay extraction based macromodel, such

as DEPACT [9], has been used to represent the interconnect in the circuit network. This section provides an overview for the MOR algorithm proposed in [14].

It has been proven in [14] that the relation between the port currents and voltages of N lossless transmission lines, can be written as

$$\boldsymbol{A}_o\boldsymbol{x}_L(t)+\sum_{k=1}^{N}\boldsymbol{A}_k\boldsymbol{x}_L(t-\tau_k) = -\boldsymbol{B}_o\boldsymbol{i}_L(t) \tag{3.27}$$

$$\boldsymbol{v}_L(t) = \boldsymbol{B}_o^T\boldsymbol{x}_L(t) \tag{3.28}$$

where $\boldsymbol{x}_L \in \mathbb{R}^{4N\times 4N}$ is the state variables of the lossy multi transmission line, $\boldsymbol{i}_L(t)$,$\boldsymbol{v}_L(t)$ are the port currents and voltages of the lossy coupled lines, respectively and

$$\boldsymbol{A}_o=\begin{bmatrix} -\frac{\boldsymbol{Z}_o}{2} & \boldsymbol{0} & \frac{\boldsymbol{Z}_o}{2} & \boldsymbol{0} \\ \boldsymbol{0} & -\frac{\boldsymbol{Z}_o}{2} & \boldsymbol{0} & \frac{\boldsymbol{Z}_o}{2} \\ -\frac{\boldsymbol{Z}_o}{2} & \boldsymbol{0} & -\frac{\boldsymbol{Z}_o}{2} & \boldsymbol{0} \\ \boldsymbol{0} & -\frac{\boldsymbol{Z}_o}{2} & \boldsymbol{0} & -\frac{\boldsymbol{Z}_o}{2} \end{bmatrix} \quad \boldsymbol{A}_k=\frac{\boldsymbol{\Gamma}}{2}\begin{bmatrix} \boldsymbol{0} & -\boldsymbol{e}_k & \boldsymbol{0} & -\boldsymbol{e}_k \\ -\boldsymbol{e}_k & \boldsymbol{0} & -\boldsymbol{e}_k & \boldsymbol{0} \\ \boldsymbol{0} & \boldsymbol{e}_k & \boldsymbol{0} & \boldsymbol{e}_k \\ \boldsymbol{e}_k & \boldsymbol{0} & \boldsymbol{e}_k & \boldsymbol{0} \end{bmatrix}\boldsymbol{\Gamma}^{-1}\boldsymbol{Z}_0 \tag{3.29}$$

$$\boldsymbol{B}_o = \begin{bmatrix} \mathbf{0} & \mathbf{0} \\ \mathbf{0} & \mathbf{0} \\ \boldsymbol{Z}_0 & \mathbf{0} \\ \mathbf{0} & \boldsymbol{Z}_0 \end{bmatrix} \tag{3.30}$$

where $\boldsymbol{e}_k \in \mathbb{R}^{N\times N}$ is a zero matrix except the (k,k) element is equal to "1", Z_0 is the characteristic impedance of the transmission line, τ_k is the delay corresponding to each line, Γ contains the Eigen vectors of the matrix $\sqrt{\boldsymbol{LC}}d$ where $\boldsymbol{L}$ and $\boldsymbol{C}$ are the p.u.l parameters of the coupled lossless transmission line.

If an RLC circuit, whose MNA equations is given by (3.3) and (3.4), is attached to coupled lossless transmission lines described by (3.27), the MNA equations of the overall network can be written in the frequency domain as [14]

$$\tilde{\boldsymbol{G}}\tilde{\boldsymbol{X}}(s) + s\tilde{\boldsymbol{C}}\tilde{\boldsymbol{X}}(s) = \sum_{k=1}^{N} \tilde{\boldsymbol{A}}_k \tilde{\boldsymbol{X}}(s) e^{-s\tau_k} + \tilde{\boldsymbol{B}}\boldsymbol{u}_{in}(s) \tag{3.31}$$

$$\boldsymbol{i}_{out}(s) = \tilde{\boldsymbol{B}}^T \tilde{\boldsymbol{X}}(s) \tag{3.32}$$

where

$$\tilde{\boldsymbol{G}} = \begin{bmatrix} \boldsymbol{G}_\phi & \mathbf{0} & \boldsymbol{P} \\ \mathbf{0} & -\boldsymbol{A}_o & -\boldsymbol{B}_o \\ -\boldsymbol{P}^T & \boldsymbol{B}_o^T & \mathbf{0} \end{bmatrix} \quad \tilde{\boldsymbol{C}} = \begin{bmatrix} \boldsymbol{C}_\phi & \mathbf{0} & \mathbf{0} \\ \mathbf{0} & \mathbf{0} & \mathbf{0} \\ \mathbf{0} & \mathbf{0} & \mathbf{0} \end{bmatrix}$$

$$\tilde{\boldsymbol{A}}_k = -\begin{bmatrix} 0 & 0 & 0 \\ 0 & -\boldsymbol{A}_k & 0 \\ 0 & 0 & 0 \end{bmatrix} \quad \tilde{\boldsymbol{B}} = \begin{bmatrix} \boldsymbol{b}_\phi \\ 0 \\ 0 \end{bmatrix} \quad \tilde{\boldsymbol{X}}(s) = \begin{bmatrix} \boldsymbol{x}_\phi(s) \\ \boldsymbol{x}_L(s) \\ \boldsymbol{i}_L(s) \end{bmatrix} \in \mathbb{R}^{\tilde{N}}$$

with $\tilde{N} = N_\phi + 6N$ and $\boldsymbol{P}$ is a selector matrix that maps the port currents of the lossless transmission lines into the node space of the RLC circuit. The admittance matrix of the above system can be written as [14]

$$\boldsymbol{Y}(s) = \tilde{\boldsymbol{B}}^T (s\tilde{\boldsymbol{C}} + \tilde{\boldsymbol{G}} - \sum_{k=1}^{N} \tilde{\boldsymbol{A}}_k e^{-s\tau_k})^{-1} \tilde{\boldsymbol{B}} \tag{3.33}$$

The major problem in (3.33) is that the moments are not related by the recursive relation shown in (3.8) and (3.9), as in the case of RLC circuits. Therefore, the Arnoldi algorithm cannot be applied to (3.33) directly. This problem can be solved by expanding the exponential matrix $e^{-s\tau_k}$ by its Taylor series as [14]

$$\left[\boldsymbol{\Psi}_0 + \boldsymbol{\Psi}_1 s + \cdots + \boldsymbol{\Psi}_{n-1} s^{n-1}\right] \boldsymbol{\Phi}(s) = \tilde{\boldsymbol{B}} \boldsymbol{u}_{in}(s) \tag{3.34}$$

where n is the number of terms required by the Taylor series so that it is a good approximation and

$$\boldsymbol{\Psi}_i = \begin{cases} \tilde{\boldsymbol{G}} - \sum_{j=1}^{N} \tilde{\boldsymbol{A}}_j \frac{(-\tau_j)^i}{i!} & i = 0 \\ \tilde{\boldsymbol{C}} - \sum_{j=1}^{N} \tilde{\boldsymbol{A}}_j \frac{(-\tau_j)^i}{i!} & i = 1 \\ -\sum_{j=1}^{N} \tilde{\boldsymbol{A}}_k \frac{(-\tau_j)^i}{i!} & i \geq 2 \end{cases} \tag{3.35}$$

Since $\boldsymbol{\Phi}(s)$ is a good approximation of $\tilde{\boldsymbol{X}}(s)$ in (3.31), the orthogonal basis that span the first q block moments of $\tilde{\boldsymbol{X}}(s)$ can be calculated from the orthogonal basis that span the first q block moments of $\boldsymbol{\Phi}(s)$. However, in order to use the Arnoldi algorithm to calculate the orthogonal basis of $\boldsymbol{\Phi}(s)$, (3.34) should be re-written as [14]

$$s\boldsymbol{\zeta}\boldsymbol{\xi}(\boldsymbol{s}) + \Lambda\boldsymbol{\xi}(\boldsymbol{s}) = \boldsymbol{\kappa}\boldsymbol{u}_{in}(s) \tag{3.36}$$

where

$$\Lambda = \begin{bmatrix} \boldsymbol{\Psi}_0 & \mathbf{0} & \dots & \mathbf{0} \\ \mathbf{0} & -\boldsymbol{I} & \mathbf{0} & \mathbf{0} \\ \vdots & & \ddots & \\ \mathbf{0} & \dots & \mathbf{0} & -\boldsymbol{I} \end{bmatrix} \qquad \boldsymbol{\zeta} = \begin{bmatrix} \boldsymbol{\Psi}_1 & \boldsymbol{\Psi}_2 & \dots & \boldsymbol{\Psi}_n \\ \boldsymbol{I} & \mathbf{0} & \dots & \mathbf{0} \\ & & \ddots & \\ \mathbf{0} & \dots & \boldsymbol{I} & \mathbf{0} \end{bmatrix} \tag{3.37}$$

$$\boldsymbol{\kappa} = \begin{bmatrix} \tilde{\boldsymbol{B}} \\ \mathbf{0} \\ \vdots \\ \mathbf{0} \end{bmatrix} \qquad \boldsymbol{\xi}(s) = \begin{bmatrix} \boldsymbol{\Phi}(s) \\ s\boldsymbol{\Phi}(s) \\ \vdots \\ s^{n-1}\boldsymbol{\Phi}(s) \end{bmatrix} \tag{3.38}$$

It was proven in [14,30] that the columns in the first $\tilde{N} \times k$ block in the orthogonal basis of the first block moments of $\boldsymbol{\xi}(s)$ in (3.36) (where k is the number of the columns of the Krylov subspace of (3.31)) will span the subspace of the moments of $\tilde{\boldsymbol{X}}(s)$. After finding the orthogonal basis $\boldsymbol{Q}$, using the block Arnoldi algorithm, the reduced system can be represented by

$$\hat{\boldsymbol{G}}\hat{\boldsymbol{x}}(t) + \hat{\boldsymbol{C}}\dot{\hat{\boldsymbol{x}}}(t) = \sum_{k=1}^{N} \hat{\boldsymbol{A}}_k \hat{\boldsymbol{x}}(t - \tau_k) + \hat{\boldsymbol{B}}\boldsymbol{u}_{in}(t) \tag{3.39}$$

$$\boldsymbol{i}_{out}(t) = \hat{\boldsymbol{B}}^T \hat{\boldsymbol{x}}(t) \tag{3.40}$$

where $\hat{\boldsymbol{G}} = \boldsymbol{Q}^T\tilde{\boldsymbol{G}}\boldsymbol{Q}$, $\hat{\boldsymbol{C}} = \boldsymbol{Q}^T\tilde{\boldsymbol{C}}\boldsymbol{Q}$, $\hat{\boldsymbol{A}}_k = \boldsymbol{Q}^T\tilde{\boldsymbol{A}}_k\boldsymbol{Q}$ and $\hat{\boldsymbol{B}} = \boldsymbol{Q}^T\tilde{\boldsymbol{B}}$.

The reduced Y-parameters matrix can be written as [14]

$$\hat{\boldsymbol{Y}}(s) = \hat{\boldsymbol{B}}^T(s\hat{\boldsymbol{C}} + \hat{\boldsymbol{G}} - \sum_{k=1}^{N} \hat{\boldsymbol{A}}_k e^{-s\tau_k})^{-1}\hat{\boldsymbol{B}} \tag{3.41}$$

The reduced Y-parameters matrix of the macromodel can be inserted in the overall MNA equations of the complete system. The steps for finding the reduced system is given in Algorithm 3 [14].

Algorithm 2 Extracting the reduced model of a network with delay elements

1: Form the matrices that form the equation (3.27)

2: Form the MNA matrices for the whole system as in (3.31)

3: Form the MNA equations after expanding the delay elements in Taylor series as in (3.34)

4: Find the Orthogonal basis of the system represented by (3.36) using the block Arnoldi algorithm

5: Extract the first $\tilde{N} \times k$ columns from the generated orthogonal basis and perform an extra orthogonalization on the extracted columns

6: Find the reduced system in (3.39)

It is to be noted that step 5 in the algorithm requires an extra orthogonalization. This extra orthogonalization is required since the first $\tilde{N} \times k$ columns will not be orthogonal.

3.5 Summary

In this chapter, multiport model order reduction algorithms have been reviewed. One of the model order reduction algorithms is AWE. AWE suffers from numerical limitations when a higher order model is required. Other reduction algorithms, such as the Krylov subspace projection methods, have been presented . These methods do not suffer from the same limitations as AWE and allow us to obtain very high reduced order models.

Projection-based algorithms are limited only to RLC circuits. A recently proposed reduction algorithm for large networks with delay elements, which overcomes the limitation in Projection-based algorithms has been reviewed.

Chapter 4

Efficient Model-Order Reduction of Multi-Port Interconnects using Conventional Lumped Segmentation

In this chapter, an efficient MOR approach is presented for large multi-port interconnects. The proposed approach improves a recently proposed MOR method [12] that exploits the WR-TP algorithm [13]. Using WR-TP, the interconnects structure is decoupled into single line subcircuits. Each individual line can be reduced using a suitable reduction algorithm, such as PRIMA [11].

Section (4.1) gives an introduction to the waveform relaxation algorithm. Section (4.2) gives an overview for the decoupling strategy that was recently proposed in [12]. A proposed time-domain approach for calculating the WR sources is presented in section (4.3). Details of the transient simulation of the reduced model are described in section (4.4). Section (4.5) provides numerical examples to validate the accuracy of the proposed approach. Section (4.6) presents a proposed parallel simulation for the proposed method.

4.1 Review of Waveform Relaxation Algorithm

Waveform relaxation (WR) has been proposed in the literature [31–35] as an alternative method to the convention time-stepping methods used for solving ordinary differential equations. In WR, the set of coupled differential equations is first partitioned into separate differential equations. An iterative process, called relaxation process, is then applied to each differential equation until the solution has converged within an acceptable error tolerance [36]. The concept of partitioning the differential equations can also be applied to the circuit level. The original circuit can be partitioned into subcircuits that are solved separately for the entire time-interval of interest. The coupling effects among these subcircuits are represented by time-domain sources called WR-sources. These sources are updated during the relaxation process until convergence is obtained.

Several WR methods have been proposed [13, 37–40] in the literature for simulating interconnect circuits. In this section, waveform relaxation based on transverse partitioning that exploits the weak coupling between the lines is reviewed.

4.1.1 Review of Transverse Partitioning

Transverse partitioning was proposed in [4, 13, 40] as an alternative method to the longitudinal partitioning. It was proven that the number of iterations required for convergence in the transverse partitioning is very few compared to the longitudinal partitioning algorithm that was initially proposed for interconnect circuits [37–39]. In this method, the coupled TLs are partitioned in the transverse direction into single lines and each line is simulated separately. The coupling effects due to the neighboring lines are represented using voltage/current sources called WR sources.

Consider the telegrapher's equations of N coupled transmission line given in (2.1). The equation of the j^{th} line can be written as [13]

$$\frac{\partial}{\partial z}v_j(z,t) = -R_{jj}i_j(z,t) - L_{jj}\frac{\partial}{\partial t}i_j(z,t) + \tilde{\eta}_j(z,t) \tag{4.1}$$

$$\frac{\partial}{\partial z}i_j(z,t) = -\hat{G}_{jj}v_j(z,t) - \hat{C}_{jj}\frac{\partial}{\partial t}v_j(z,t) + \tilde{\gamma}_j(z,t) \tag{4.2}$$

where $\hat{C}_{jj} = \sum_{k=1}^{N} C_{jk}$, $\hat{G}_{jj} = \sum_{k=1}^{N} G_{jk}$, and $\tilde{\eta}_j(z,t)$, $\tilde{\gamma}_j(z,t)$ are the coupling effects

from the neighboring lines and they are defined as

$$\tilde{\eta}_j(z,t) = -\sum_{\substack{k=1 \\ k\neq j}}^{N} \left(R_{jk} i_k + L_{jk} \frac{\partial i_k}{\partial t} \right) \tag{4.3}$$

$$\tilde{\gamma}_j(z,t) = -\sum_{\substack{k=1 \\ k\neq j}}^{N} \left(G_{jk} v_{jk} + C_{jk} \frac{\partial v_{jk}}{\partial t} \right) \tag{4.4}$$

where $i_k = i_k(z,t)$, $v_k = v_k(z,t)$ and $v_{jk} = v_j - v_k$

In (4.1) and (4.2), the only unknown variables are the voltage and the currents of the j^{th} line (assuming that $\tilde{\eta}_j(z,t)$ and $\tilde{\gamma}_j(z,t)$ are known). Therefore, the coupled partial differential equations in (4.1) and (4.2) can be decoupled using the waveform relaxation algorithm as follows [13]

$$\frac{\partial}{\partial z} v_j^{(r+1)}(z,t) = -R_{jj} i_j^{(r+1)}(z,t) - L_{jj} \frac{\partial}{\partial t} i_j^{(r+1)}(z,t) + \tilde{\eta}_j^{(r)}(z,t) \tag{4.5}$$

$$\frac{\partial}{\partial z} i_j^{(r+1)}(z,t) = -\hat{G}_{jj} v_j^{(r+1)}(z,t) - \hat{C}_{jj} \frac{\partial}{\partial t} v_j^{(r+1)}(z,t) + \gamma_j^{(r)}(z,t) \tag{4.6}$$

where r represents the r^{th} iteration.

The coupling effects between the lines can be represented by voltage and current sources attached to each line (Henceforth, referred to as *WR sources*). Two approaches have been proposed in [13] for computing the WR sources. The first approach is the single-ended representation, where the coupling effects are represented by voltage and current sources that are located at the end of each line. This approach presents the basis for the decoupling strategy of the previously proposed MOR method [12]. The second approach is the distributed representation. In this

approach the coupling effects are represented by voltage and current sources that are distributed throught the decoupled lines and are connected at the end of each lumped segment.

First, a brief overview of the single ended representation and the previously proposed decoupling strategy are presented. Next, details of the proposed method for calculating the WR-sources, which is based on the distributed sources representation, are given.

4.2 Review of the Decoupling Strategy

In this section, a brief overview for the WR-TP based decoupling strategy that was proposed in [12] is given. In WR-TP, the N coupled transmission line circuit is partitioned into N single line subcircuits. The coupling effects due to neighboring lines are represented using voltage and current sources. Since the multiport interconnect structure is decoupled into single lines subcircuit, MOR can be applied to each line independently.

The coupling effects given in (4.3) and (4.4) can be represented in the frequency domain at the r^{th} iteration as [13]

$$\begin{bmatrix} \eta_j^{(r)}(d,s) \\ \gamma_j^{(r)}(d,s) \end{bmatrix} = \int_0^d e^{F_j(d-\lambda)} \Psi_j^{(r)}(\lambda,s) d\lambda \tag{4.7}$$

where

$$F_j = \begin{bmatrix} 0 & -R_{jj} - sL_{jj} \\ -G_{jj} - sC_{jj} & 0 \end{bmatrix} \tag{4.8}$$

$$\Psi_j^{(r)}(z,s) = \sum_{\substack{k=1 \\ k \neq j}}^{N} \begin{bmatrix} 0 & -R_{jk} - sL_{jk} \\ -G_{jk} - sC_{jk} & 0 \end{bmatrix} \begin{bmatrix} V_{jk}^{(r)}(z,s) \\ I_k^{(r)}(z,s) \end{bmatrix} \tag{4.9}$$

Equation (4.10) represents the basis for updating the WR-sources at the r^{th} iteration. Using (4.7-4.10), the coupling effects can be modeled as voltage and current sources connected to the far-end of each line as shown in Fig. 4.1. It is to be noted that the WR-sources in (4.7) can be calculated analytically using an integration formula, such as trapezoidal rule [13].

$$\begin{bmatrix} \eta_j^{(r)}(z+\Delta z, s) \\ \gamma_j^{(r)}(z+\Delta z, s) \end{bmatrix} = e^{F_j \Delta z} \begin{bmatrix} \eta_j(z,s) \\ \gamma_j(z,s) \end{bmatrix} + \frac{\Delta z}{2} \left[e^{\Delta z} \Psi_j(z,s) + \Psi_j(z+\Delta z, s) \right] \tag{4.10}$$

Using the single ended representation, model order reduction can be applied to each line separately using the Krylov projection method. Fig 4.1 shows the steps for applying MOR on interconnects using WR-TP, as proposed in [12].

As shown in (4.7) the WR sources are calculated in the frequency domain, which may be inefficient when simulating very large interconnects circuits due to the need of FFT/IFFT at each iteration. In the next section, a proposed time-domain approach

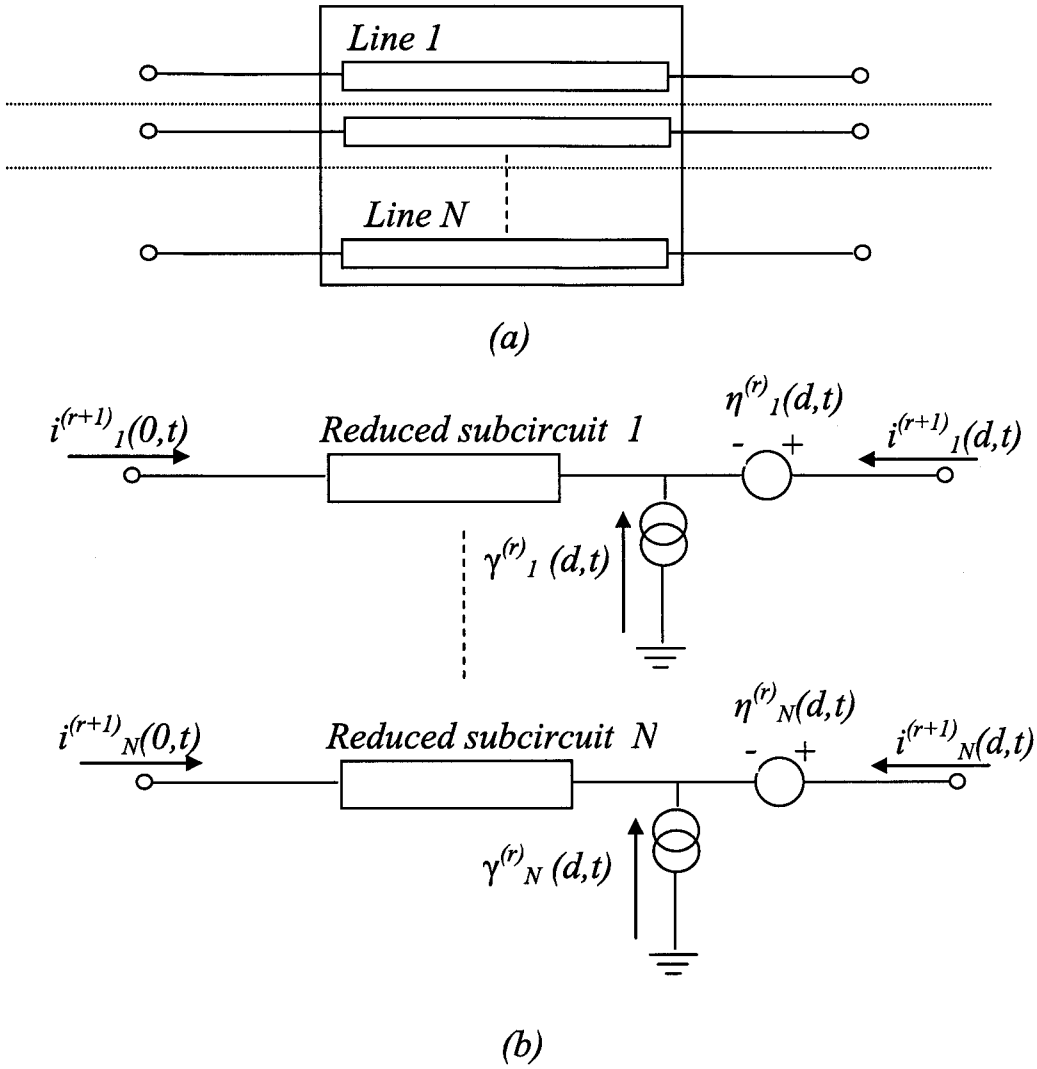

Figure 4.1: a) Applying WR-TP to the interconnects structure b)Reducing each line separately

for calculating the WR sources, which is based on the distributed sources approach is presented.

4.3 Proposed Time-Domain Approach for Calculating the WR Sources

The proposed method for calculating the WR sources [41] is based on the distributed representation [13] of the relaxation sources. In this representation the relaxation sources are added after each lumped section of the transmission line macromodel. Consider the integral form of the WR sources in (4.7). This integration can be discretized as follows [13]

$$\eta_j(z_n,t) = -w_n \Delta z_n \sum_{\substack{k=1 \\ k\neq j}}^{N} \left(R_{jk} i_k(z_n,t) + L_{jk} \frac{\partial}{\partial t} i_k(z_n,t) \right) \tag{4.11}$$

$$\gamma_j(z_n,t) = -w_n \Delta z_n \sum_{\substack{k=1 \\ k\neq j}}^{N} \left(G_{jk} v_k(z_n,t) + C_{jk} \frac{\partial}{\partial t} v_k(z_n,t) \right) \tag{4.12}$$

where w_n is a weighting factor, m is the number of discretization points (i.e. number of sections), z_n is the distance from the near-end of the line and $\Delta z_n = z_n - z_{n-1}$.

It was shown in [13] that (4.11) and (4.12) can be represented as voltage and current sources attached at distance z_n. Fig. 4.2 shows the distributed source approach used with conventional lumped segmentation macromodel.

Since the distributed WR sources can be calculated directly in the time domain ,as shown in (4.11) and (4.12), they will be used in this section to represent the coupling

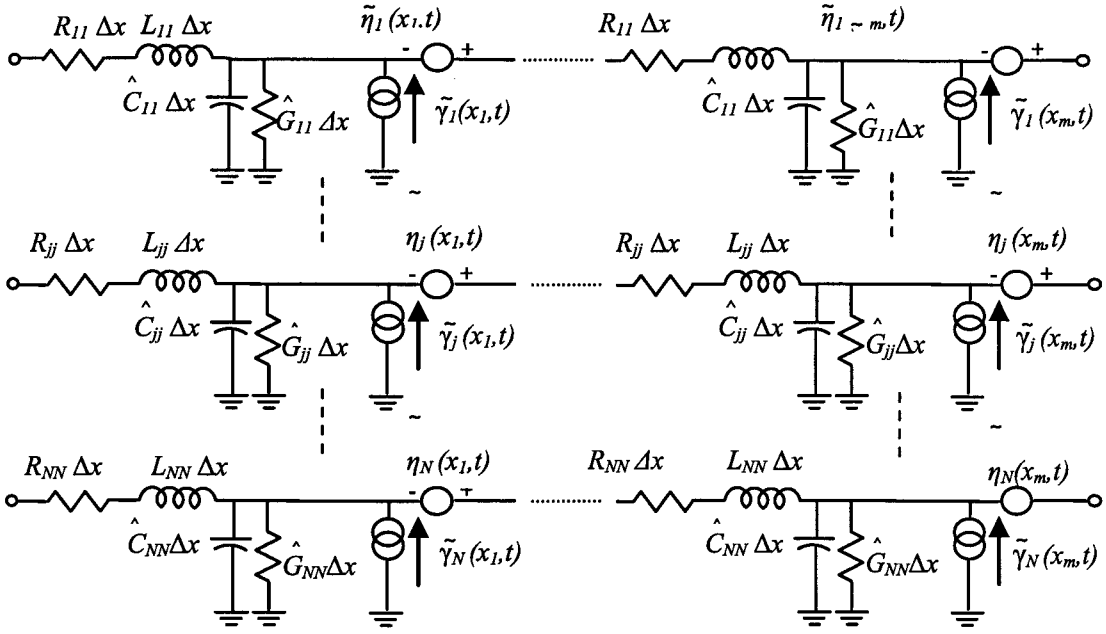

Figure 4.2: Distributed sources added after each lumped Section [4]

between the lines. However, the number of independent voltage/current sources in this circuit will be extremely large due to the distributed WR sources that were added after each section of the lumped model. Hence, directly applying the block Arnoldi algorithm [29] to each line in order to find an orthogonal projection matrix $\boldsymbol{Q}$ will be inefficient and can result in a very large matrix.

To overcome this problem, the distributed WR-sources are replaced by two voltage sources that are attached to the terminals of each line. These equivalent sources are derived using the generalized Thevenin theorem for an active two port network [42] (Henceforth, referred to as *Thevenin sources*).

Since, the Thevenin sources are used to replace the distributed WR-sources, the

MNA equations of the j^{th} line can be re-written as

$$\boldsymbol{C}_{\phi j}\,\dot{\mathbf{x}}_{\phi j}^{(r+1)}(t) + \boldsymbol{G}_{\phi j}\,\mathbf{x}_{\phi j}^{(r+1)}(t) = \boldsymbol{b}_{\phi j}\,\boldsymbol{u}_{in\,j}^{(r+1)}(t) + \boldsymbol{d}_{\phi j}\begin{bmatrix} \boldsymbol{E_{Aj}}^{(r)}(t) \\ \boldsymbol{E_{Bj}}^{(r)}(t) \end{bmatrix} \tag{4.13}$$

where

- r represents the r^{th} iteration in the WR-TP algorithm.
- $\boldsymbol{x}_{\phi j}^{(r+1)} \in \mathbb{R}^{N_{\phi j}}$ is the vector of node voltage waveforms and current waveforms of the j^{th} line,
- $\boldsymbol{d}_{\phi j} \in \mathbb{R}^{N_{\phi j} \times 2}$ is a selector matrix that maps the Thevenin sources of the j^{th} line into the node space of the line,
- $\boldsymbol{E}_{Aj}^{(r)}$, $\boldsymbol{E}_{Bj}^{(r)}$ contain the values of the Thevenin sources of the j^{th} line, as shown in Fig. 4.4.

The Thevenin sources are calculated by finding the open circuit voltages at the two ports of the line after removing all line terminations, as shown in Fig. 4.3. It is to be noted that the computational cost of calculating the Thevenin sources is equal to solving a sparse linear matrix representing the line.

The MNA equations of each line (4.13) can be reduced by transforming $\boldsymbol{x}_{\phi j}$ to $\hat{\boldsymbol{x}}_{\phi j}$ using the PRIMA algorithm. The reduced-order MNA equations can be expressed as

$$\hat{C}_{\phi j}\,\dot{\hat{\mathbf{x}}}_j^{(r+1)}(t) + \hat{G}_{\phi j}\,\hat{\mathbf{x}}_{\phi j}^{(r+1)}(t) = \hat{b}_{\phi j}\,u_{in\,j}^{(r+1)}(t) + Q_j^T\,d_{\phi j}\begin{bmatrix} E_{Aj}^{(r)}(t) \\ E_{Bj}^{(r)}(t) \end{bmatrix} \tag{4.14}$$

where

$$\begin{aligned} x_{\phi j} &= Q_j \hat{x}_{\phi j} \\ \hat{G}_{\phi,j} &= Q_j{}^T G_{\phi,j} Q_j \\ \hat{C}_{\phi,j} &= Q_j{}^T C_{\phi,j} Q_j \\ \hat{b}_{\phi,j} &= Q_j{}^T b_{\phi,j} \end{aligned} \tag{4.15}$$

(4.16)

In the case of N coupled lines interconnects, the reduced model consists of N single line reduced subcircuits, each described by (4.14).

4.4 Transient Analysis of the Reduced Model

At a given iteration, the transient simulation of the overall network including the coupled interconnects is performed by embedding the reduced set of equations (4.15) into the MNA equations of the overall network. The resulting equations are solved using any of the conventional time domain circuit simulation techniques [12]. In order to update the WR sources in (4.11) and (4.12), the internal voltages and currents $v_{jk}(x_n,t)$ and $i_k(x_n,t)$ (for $j,k = 1,\ldots,N\ k \neq j$), are required. However, since

the overall circuit has been simulated using the reduced model, these voltages and currents are not readily available. A straight forward approach to calculate the internal voltages and currents is by re-simulating the circuit in Fig. 4.3, where E_{Aj} and E_{Bj} are replaced by the port voltage waveforms obtained from the simulation of the overall circuit (using the reduced model), and where the distributed WR sources are from the previous iteration. However, this step could be avoided by using the following proposition.

Proposition 1: The currents and voltages required to update the WR sources in (4.11) and (4.12) (i.e. $i_k(z_n,t)$ and $v_{jk}(z_n,t)$, as in Fig. 4.5) can be calculated as follows.

$$\begin{aligned} i_k^{(r)}(z_n,t) &= i_{k,th}^{(r)}(z_n,t) + i_{k,oc}^{(r)}(z_n,t) \\ v_{jk}^{(r)}(z_n,t) &= v_{jk,th}^{(r)}(z_n,t) + v_{jk,oc}^{(r)}(z_n,t) \\ j,k &= 1 \ldots N \quad k \neq j \end{aligned} \tag{4.17}$$

where $i_{k,th}^{(r)}$, $v_{jk,th}(z_n,t)^{(r)}$ are the currents and voltages obtained while simulating the k^{th} line with the Thevenin sources, as shown in Fig. 4.4 and $i_{k,oc}^{(r)}$, $v_{jk,oc}(z_n,t)^{(r)}$ are the currents and voltages obtained while simulating the k^{th} line without terminations to find the Thevenin equivalent sources as shown in Fig. 4.3. The proof of the *proposition1* is given as follows [41]

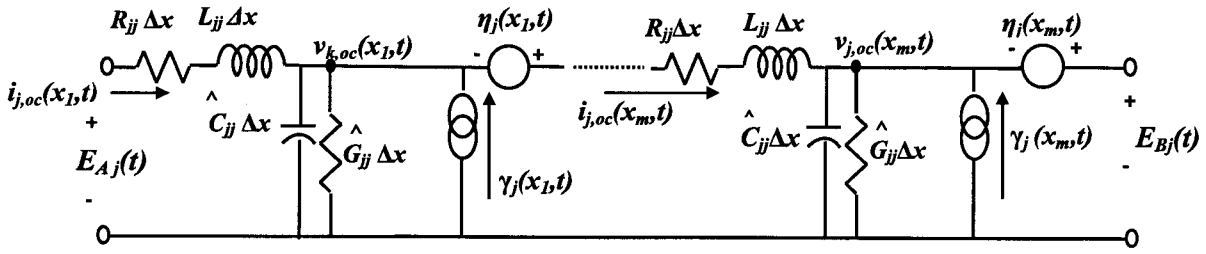

Figure 4.3: The equivalent circuit of the j^{th} line when the terminations are removed to find the Thevenin sources

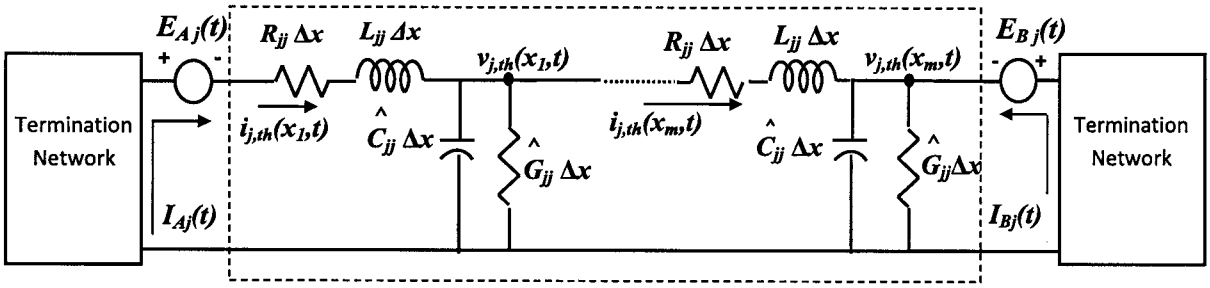

Figure 4.4: Replacing the distributed sources with Thevenin equivalent sources

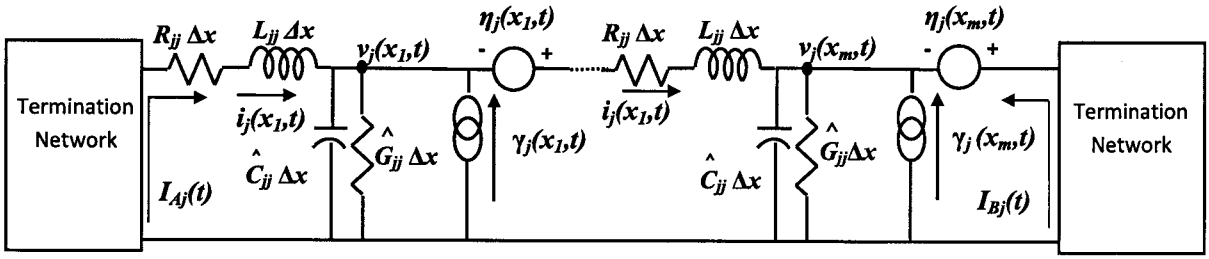

Figure 4.5: The Original circuit of the j^{th} line if the distributed WR sources are used

proof: Consider the three circuits shown in Fig. 4.3-4.5. Since the circuits shown in Fig. 4.4 and Fig. 4.5 will have the same currents flowing through the terminal circuits $(I_{A_k}(t), I_{B_k}(t))$, the terminal circuits can be replaced by two current sources that have the same values of the currents (substitution Theorem). Therefore, without the loss of generality, the MNA equations of the circuit shown in Fig. 4.5 can be written in the frequency domain, using the superposition theorem as,

$$\boldsymbol{X}(s) = \boldsymbol{Y}^{-1} \begin{bmatrix} \boldsymbol{\eta_k}(s) \\ \boldsymbol{\gamma_k}(s) \end{bmatrix} + \boldsymbol{Y}^{-1} \begin{bmatrix} I_{A_k}(s) \\ I_{B_k}(s) \end{bmatrix} \tag{4.18}$$

where $\boldsymbol{Y} = (\boldsymbol{G} + s\boldsymbol{C})$ and $\boldsymbol{\eta_k}, \boldsymbol{\gamma_k}$ are vectors that contain the values of the distributed sources.

The first term in the right hand side of (4.18) is equivalent to simulating the k^{th} line with the WR sources and open circuit terminations, as shown in Fig. 4.3. The second term is equivalent to simulating the k^{th} line with the terminations and Thevenin sources, as shown in Fig. 4.4.

Therefore the currents/voltages required to update the WR sources can be written as the sum of the currents/voltages of the k^{th} line when simulated without terminations, and the currents/voltages of the k^{th} line when simulated with the Thevenin sources (4.17).

□

It is worth noting that $i_{k,th}^{(r)}$, $v_{jk,th}(z_n,t)^{(r)}$ can be calculated from the reduced model using (4.15) as

$$\begin{aligned} i_{k,th}^{(r)}(z_n,t) &= \alpha_n \boldsymbol{Q}_k \hat{\boldsymbol{x}}_{\phi k}^{(r)} \\ v_{jk,th}^{(r)}(z_n,t) &= \beta_n(\boldsymbol{Q}_j \hat{\boldsymbol{x}}_{\phi j}^{(r)} - \boldsymbol{Q}_k \hat{\boldsymbol{x}}_{\phi k}^{(r)}) \end{aligned} \tag{4.19}$$

where α_n,β_n are selector matrices.

The WR sources can be calculated as

$$\begin{aligned} \eta_j(z_n,t) &= -w_n \Delta z_n \sum_{\substack{k=1 \\ k\neq j}}^{N} \Bigg(R_{jk}\Big(\alpha_n \boldsymbol{Q}_k \hat{\boldsymbol{x}}_{\phi k}^{(r)} + i_{k,oc}^{(r)}(z_n,t)\Big) \\ &+ L_{jk}\frac{\partial}{\partial t}\Big(\alpha_n \boldsymbol{Q}_k \hat{\boldsymbol{x}}_{\phi k}^{(r)} + i_{k,oc}^{(r)}(z_n,t)\Big)\Bigg) \end{aligned} \tag{4.20}$$

$$\begin{aligned} \gamma_j(z_n,t) &= -w_n \Delta z_n \sum_{\substack{k=1 \\ k\neq j}}^{N} \Bigg(G_{jk}\Big(\beta_n(\boldsymbol{Q}_j \hat{\boldsymbol{x}}_{\phi j}^{(r)} - \boldsymbol{Q}_k \hat{\boldsymbol{x}}_{\phi k}^{(r)}) + v_{jk,oc}^{(r)}(z_n,t)\Big) \\ &+ C_{jk}\frac{\partial}{\partial t}\Big(\beta_n(\boldsymbol{Q}_j \hat{\boldsymbol{x}}_{\phi j}^{(r)} - \boldsymbol{Q}_k \hat{\boldsymbol{x}}_{\phi k}^{(r)}) + v_{jk,oc}^{(r)}(z_n,t)\Big)\Bigg) \end{aligned} \tag{4.21}$$

Using (4.20) and (4.21), the WR sources can be updated for the next iteration. The pseudo-code shown in Algorithm 4 summarize the computational steps of the proposed method.

Algorithm 4 The proposed coupled multi-port interconnects reduction method

1: Decouple the interconnect circuit using WR-TP

2: Find the reduced system by reducing each line individually using PRIMA.

3: Iteration $\leftarrow$ 0

4: Assume initial values for the distributed sources

5: **while** No Convergence **do**

6: Simulate each line with no terminations to obtain the open circuit voltages E_A and E_B and save the internal voltages/currents of the line.

7: Replace the distributed sources with Thevenin equivalent sources at the ports.

8: Simulate each reduced line separately with the terminations.

9: Calculate the current and voltages required to update the WR sources using (4.17) and (4.19)

10: Update the WR sources using (4.20) and (4.21)

11: iteration $\leftarrow$ iteration+1

12: **end while**

4.5 Numerical Examples

In this section, three examples are presented to demonstrate the efficiency and the speedup of the proposed method. The CPU time of the proposed algorithm is compared with the conventional MOR and Direct LU methods. All examples were simulated using a custom inhouse circuit simulator. The simulator uses the KLU package [43] to solve the circuit MNA equations. The custom simulator was used to avoid the communication with external simulator during the calculation of the WR-sources. The examples were run on Linux platform with Intel(R) Core(TM)2 Quad core processor (2.4 GHZ). In addition, the line parameters used were extrapolated based on the transmission line data provided in [44].

4.5.1 Example 1

To show the accuracy and the CPU speedup of the proposed method, we consider an interconnect network (modeled using uniform lumped segmentation) with linear termination of 50 Ω resistor at the near-end 1 pf capacitor at the far-end. The number of lines is varied between 5 and 120. The length of each line in the interconnect structure is 15 cm. Every fourth line was excited with a trapezoidal pulse current source. The rise/fall time of the source is 0.1 ns, the pulse width is 10ns and the magnitude of the pulse is 0.06 A. The number of the lumped RLC sections for each line was estimated to be 100 [2] for this example. The simulation converged to exact

answer in 4 WR iterations and 10 block-moments were required for a good accuracy.

Fig. 4.6 shows the CPU time taken to perform the transient simulation on the original coupled lines, the time to simulate the reduced circuit using conventional MOR and the time taken to find the transient response using the proposed method. It can be seen that the CPU time of the proposed method grows only linearly with the number of lines compared to an exponential growth in the conventional MOR algorithm.

To validate the accuracy of the proposed method, 50 coupled lines were considered. Fig. 4.8 shows the time-domain response (after 4 iterations) of victim line 3 at the near and far-ends respectively. The response is compared with the time-domain response of the original coupled circuit with and without reduction.

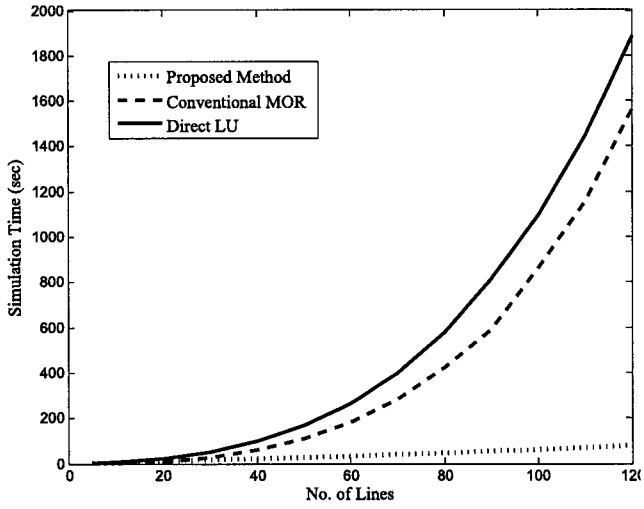

Figure 4.6: CPU time comparison

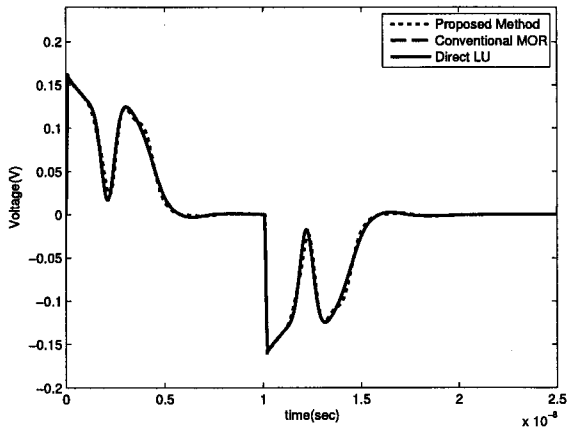

Figure 4.7: Near-end transient response of line 3 in 50 coupled lines (Example 1)

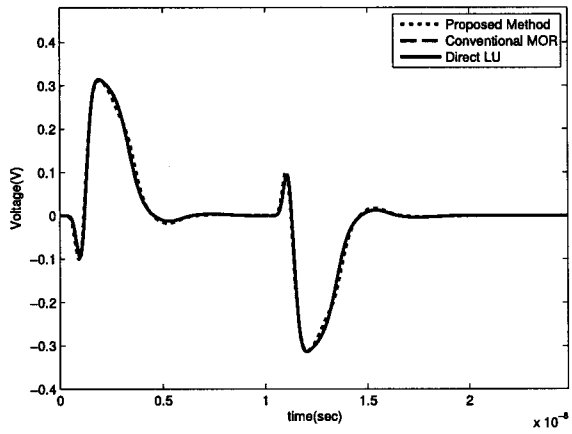

Figure 4.8: Far-end transient response of line 3 in 50 coupled lines (Example 1)

4.5.2 Example 2

To demonstrate the efficiency and the speedup of the proposed method when handling large interconnect networks, the circuit shown in Fig. 4.9 is considered. Each interconnect structure consists of 64 transmission lines of length 12 cm.

The same excitation of *Example*1 is used. The lines were modeled using 75 lumped

sections. In addition, 8 block moments were used for the model order reduction. The size of the original MNA equations is 43614, while the reduced model of the proposed method consists of 64 decoupled subcircuits for each segment, each of size 16.

Fig. 4.10 shows the far-end of line 2 in segment 3 compared to the time-domain response obtained using the Direct LU of full coupled circuit without reduction, and the time-domain response obtained using conventional MOR. As shown, the results are in good agreement. The CPU time for the proposed method was only 1.15 mins while the CPU time of the Direct LU of the full coupled circuit was 13.91 mins and conventional MOR was 4.42 mins.

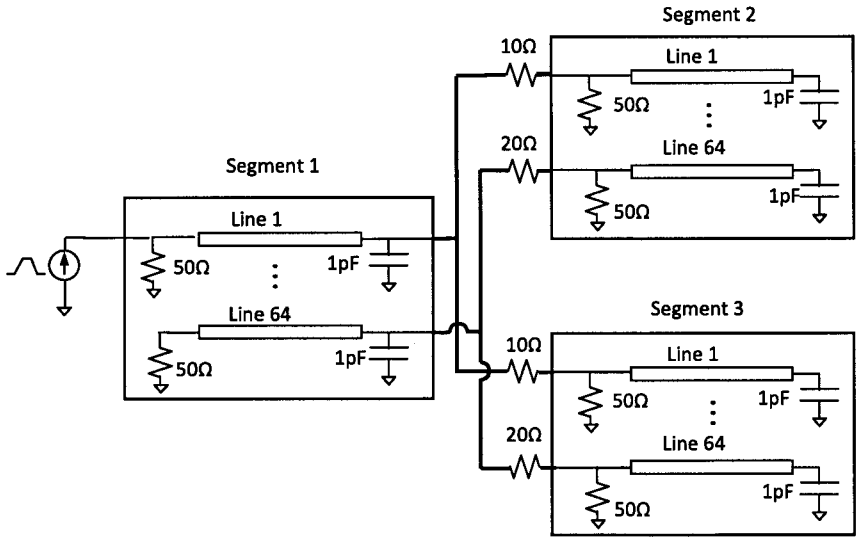

Figure 4.9: Large interconnect network (Example 2)

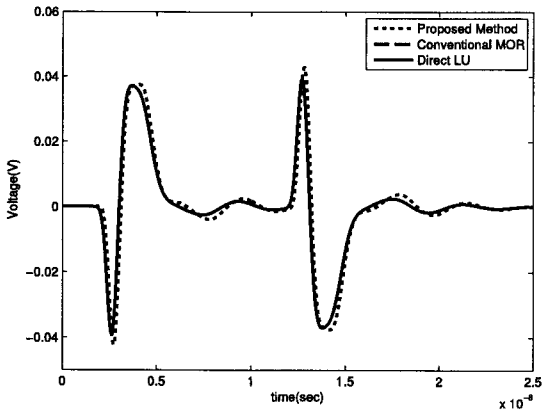

Figure 4.10: Far-end response of line 2 in segment 3 (Example 2)

4.5.3 Example 3

In this example, we show the accuracy of the proposed method when it is used to simulate coupled lines with non-linear terminations. The circuit in Fig. 4.11 was considered. The circuit consists of 24 coupled lines of length 15 cm. CMOS inverters terminate the near-ends of every fifth line. The network is excited with a trapezoidal pulse voltage source. The rise/fall time of the source is 0.1 ns, the pulse width is 10ns and the magnitude of the pulse is 1.8 V.

The lines were modeled with uniform lumped segmentation (100 sections). The number of block moments needed for a good accuracy is 10. The size of the original MNA equations is 7347, while the reduced model of the proposed method consists of 24 decoupled subcircuits each of size 34. The CPU time for the proposed method was only 18.1 secs while the CPU time of the Direct LU of the full coupled circuit was 64.95 and conventional MOR was 36.71 secs. Fig. 4.12 shows the response of the

far-end of line 10 after 4 WR iterations. As shown, the results are in an excellent agreement.

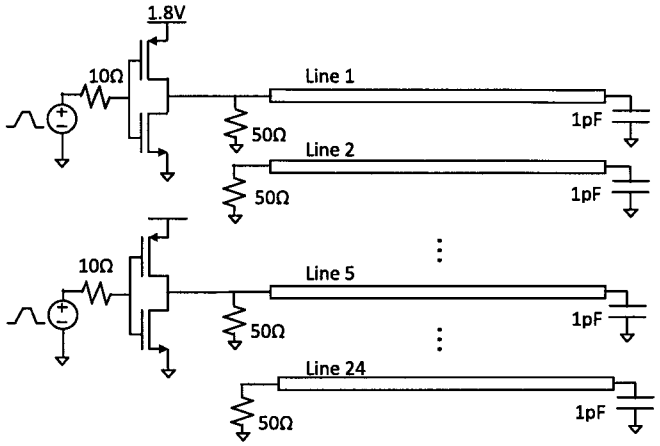

Figure 4.11: Interconnect network with non-linear terminations (Example 3)

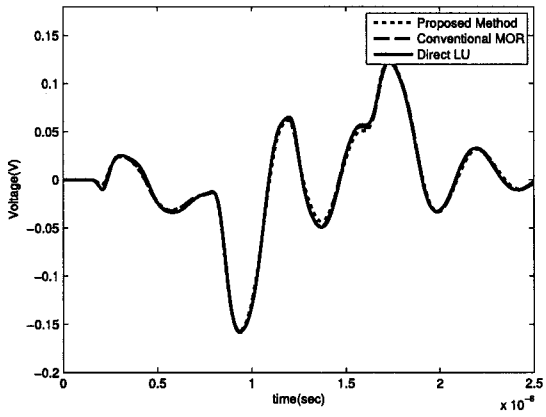

Figure 4.12: Time-domain response of line 10 far-end (Example 3)

4.5.4 Example 4

In this example, we compare the CPU time of proposed method to WR-TP method in two different situations. First, transverse partitioning is applied such that each subcircuit contains a single line. Next, we consider the case if there exists a strong coupling between the lines or if the near/far ends of the lines are attached to the same driver/reciever. In this case, applying transverse partitioning results in subcircuits that contain more than one line. In order to illustrate this situation, transverse parititioning is applied to the circuit such that each subcircuit contains 5 coupled lines.

Consider the circuit in *Example 3* with a 50 coupled lines. Table 4.1 shows the CPU time of the proposed method as compared to the WR-TP algorithm. As shown, the CPU time of WR-TP is smaller than the proposed method in the case of a single line subcircuit. However, in the case of 5 lines subcircuit, the CPU time of the proposed method is smaller than WR-TP. This is due to the fact that it is very easy to simulate a single line due to the high sparsity pattern of the MNA equations of a single line. However, in the case of 5 lines in each subcircuit, it is more effecient to simulate the reduced subcircuit than simulating the full coupled 5 lines.

	WR-TP (secs)	Proposed method (secs)
1 line/subcircuit	32.01	35.38
5 lines/subcircuit	111.91	48.04

Table 4.1: CPU time comparison of Example 4

4.6 Parallel Implementation of the Proposed Method

In this section, a parallel simulation of the proposed approach is presented. First, the calculation of the reduced model and the simulation of each line are executed in parallel. The WR sources are then updated using the voltage and currents of all the lines. Next, the WR sources are used to calculate the equivalent Thevenin sources (E_{Aj} and E_{Bj}) for each line in parallel. Once all the lines are simulated and the Thevenin sources are updated, the next iteration can begin. Algorithm 5 shows the parallel implementation of the proposed method.

Algorithm 5 Parallel implementation of the proposed method

1: Decouple the interconnect circuit using WR-TP

2: **For** each line **{ In parallel do**

3: Find the reduced model of the line using PRIMA.

4: **}**

5: Iteration $\leftarrow$ 0

6: Assume initial values for the distributed sources

7: **while** No Convergence **do**

8: **For** each line **{ In parallel do**

9: Simulate the line with no terminations to obtain the open circuit voltages E_A

and E_B and save the internal voltages/currents of the line.

10: Replace the distributed sources with Thevenin equivalent sources of the line.

11: Simulate the line with the terminations.

12: }

13: **Wait until all the lines are done**

14: **For** each line **{ In parallel do**

15: Calculate the current and voltages required to update the WR sources using (4.17) and (4.19)

16: Update the WR sources using (4.20) and (4.21)

17: }

18: iteration ← iteration+1

19: **end while**

Two examples are presented to demonstrate the performance of the parallel simulation of the proposed approach. The first example demonstrates the speedup and the CPU scalability of the parallel simulation of the proposed method for a circuit containing interconnects with uniform terminations. The second example presents the performance of the algorithm while handling the case of differing terminations. Both examples are simulated with a parallel implementation using the OpenMP multithreading library in C++.

4.6.1 Example 5

In this example, we consider an interconnect network consisting of 50 coupled lines. Each line is terminated by a 50 Ω resistor at the near-end and a 1 pf capacitor at the far-end. The lines have the same p.u.l parameters used in Example 1 and are modeled using uniform lumped segmentation. The number of sections required was 100 sections and 10 block moments were required to accurately represent each line. Each 5^{th} line is excited with same voltage source used in Example 1. The simulation was run on a dual quad-core AMD Opteron 2344HE machine.

The example was run with a varying number of processors (i.e. from 1 to 8 processors). Table 4.2 shows the CPU time of the parallel simulation of the proposed method as compared to the conventional MOR algorithm, as well as the speedup compared to the serial simulation. As shown, the parallel simulation provides a significant speedup, compared to conventional MOR, as the number of processors increases.

Fig. 4.13 shows the speedup characteristics of this example as compared to the serial simulation. An important observation is that the speedup performance moves closer to the ideal curve when the number of lines is divisible by the number of processors. For example, in the case of 5 CPUs the speedup was 4.79, which is close to the ideal speedup of 5. However, in case of 4 and 6 CPUs the speedup curve moves away from the ideal speedup curve.

#CPU	CPU time (sec)	Speedup	
		Compared to conventional MOR	Compared to serial simulation
1	23.01	4.63	1
2	13.43	7.82	1.71
3	9.5	11.22	2.42
4	6.76	15.78	3.40
5	4.8	22.22	4.79
6	4.4	24.24	5.22
7	4.24	25.16	5.42
8	3.39	33.44	6.78

Table 4.2: The CPU time comparison of the parallel simulation (Example 4)

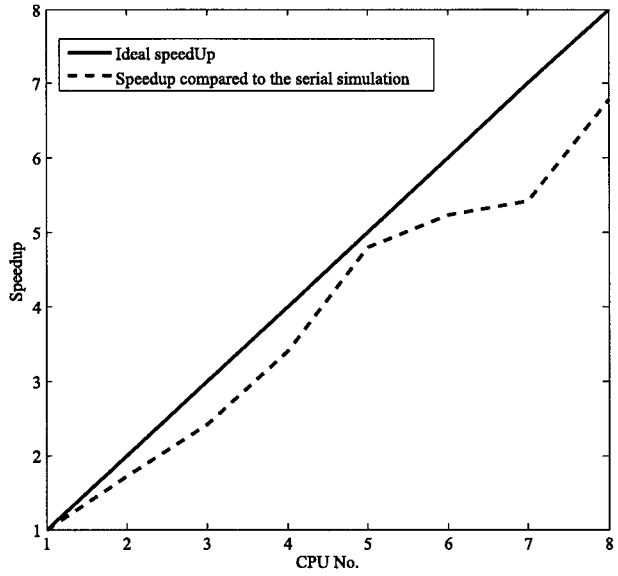

Figure 4.13: Speedup characteristics of Example 4

4.6.2 Example 6

In this example, we consider a circuit of interconnects with differing terminations. The same circuit in Example 3, which is shown in Fig. 4.11, is considered . As shown, each fourth line is terminated by a non-linear termination, while the other

lines are terminated by a linear termination.

Table 4.3 shows the speedup characteristics of this example. As expected, the speedup curve again moves closer to the ideal speedup line when the number of lines is divisible by the number of CPUs, Fig. 4.14. However, the speedup decreases as compared to example 4. This decrease in the speedup is related to the fact that the time required to simulate the lines with linear terminations is smaller than the lines with non-linear terminations. All of the line simulations must complete before moving on to the task of updating the WR-sources. Thus, the CPUs responsible for simulating the lines with linear terminations will set idle for a time after simulations are complete.

#CPU	CPU time (sec)	Speedup	
		Compared to conventional MOR	Compared to serial simulation
1	29.3	3.64	1
2	17.49	6.09	1.67
3	12.20	8.74	2.40
4	10.147	10.51	2.88
5	7.719	13.82	3.79
6	6.244	17.08	4.69
7	5.748	18.55	5.09
8	3.812	27.98	7.68

Table 4.3: The CPU time comparison of the parallel simulation (Example 5)

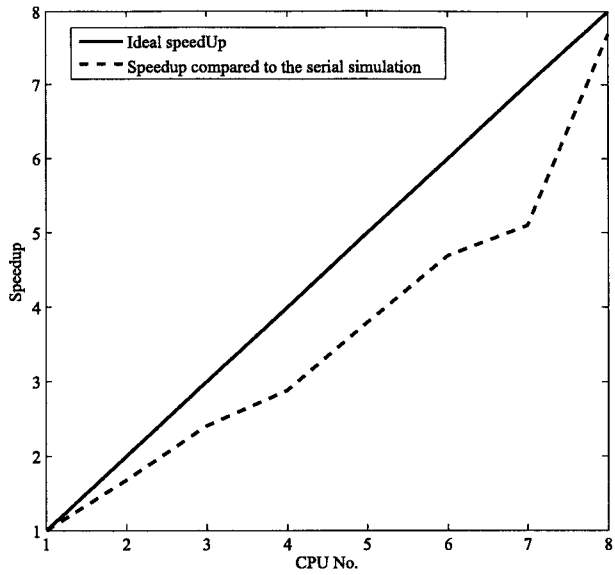

Figure 4.14: Speedup characteristics of Example 5

4.7 Summary

In this chapter, an efficient model-order reduction method for multi-port interconnects has been proposed. This method improves on a recently proposed method in [12]. A new technique for updating the WR sources directly in the time-domain has been presented. In addition, a parallel implementation has been presented. It was shown that the speedup increases significantly when the number of CPUs increases.

Chapter 5

Passive Model-Order Reduction of Multi-Port Interconnects Modeled as DEPACT Sections

In this chapter, an efficient MOR algorithm for simulation of large coupled interconnects modeled as DEPACT sections is presented. Using this algorithm, The coupled lines are partitioned into single line subcircuits. Model order reduction is then applied to each subcircuit separately. However, model order reduction algorithms, such as PRIMA, cannot be directly used to reduce each single line due to the presence of delay elements. Therefore, the reduction method proposed in [14] (reviewed in chapter 3) is used to reduce each line.

Section (5.1) gives a brief introduction. Section (5.2) provides a background for WR-TP when applied to DEPACT macromodel. Section (5.3) introduces the decoupling strategy for the multiport interconnects based on the generalized Thevenin theorem for active circuits. Section (5.4) provides the formulation of the reduced model for each decoupled line. Section (5.5) describes the source calculation algorithm and section (5.6) provides numerical examples to validate the accuracy of the new method.

5.1 Introduction

A WR-TP based MOR algorithm has been presented in chapter 4. Using this algorithm, the N coupled transmission lines are partitioned into N single lines and the coupling effects due to the neighboring lines are represented using voltage/current sources attached to each independent line. It was shown that the CPU time of the new algorithm grows linearly with the number of lines [12].

In the algorithm presented in chapter 4, the conventional lumped segmentation macromodel has been used to represent the transmission line behavior during the simulation. However, this algorithm is not limited to a specific transmission line macromodel. In this chapter, DEPACT macromdel will be used during the transient simulation of the transmission lines. The DEPACT [9] macromodel is suitable for relatively long lines. Moreover, the number of sections required in DEPACT model

is relatively small. Hence, few number of WR sources are required. It is to be noted that the proposed method is highly parallelizable due to the fact that the coupled lines are partitioned into separate single lines. Thus, array of processors can be used to simulate the decoupled lines in parallel.

The algorithm is started by partitioning the N coupled lines into N single line subcircuits, and the coupling effects due to neighboring lines are represented using voltage and current sources (WR sources). Next, the relaxation sources are replaced by Thevenin equivalent sources. Then, each line is reduced using order reduction algorithm suitable for circuits with delay elements [14]. The values for the WR sources are updated using the voltages and currents throughout each line. This process is repeated until convergence to a required accuracy is achieved. First, we will give a brief overview of the WR-TP using the DEPACT macromodel. Next, a decoupling strategy based on the generalized Thevenin theory for active circuits is presented.

5.2 Review of WR-TP Using DEPACT Macromodel

The DEPACT macromodel requires less number of sections compared to the lumped segmentation macromodel. Hence, less number of WR sources will be required when distributed sources approach is required. Moreover, when applying WR to DEPACT macromodel, the WR sources have a direct representation in time domain and no FFT/IFFT is required to update the sources [4].

Since, the DEPACT macromodel section consists of lossy and lossless parts, WR sources will be required after each part. First, evaluating the WR sources for the lossy section will be presented. Next, we present the WR sources calculation for the lossless part.

5.2.1 Waveform Relaxation Sources of the Lossy section

In this section, we give a brief overview for calculating the WR sources for the DEPACT macromodel lossy section [4]. Consider a coupled interconnects structure with a frequency-independent RLGC parameters. In this case, the DEPACT lossy section can be represented by a pure resistive network [9]. The DEPACT lossy section equation can then be written using the Y-parameters form as

$$\begin{bmatrix} \boldsymbol{i}(l_0,t) \\ \boldsymbol{i}(l_m,t) \end{bmatrix} = \boldsymbol{Y} \begin{bmatrix} \boldsymbol{v}(l_0,t) \\ \boldsymbol{v}(l_m,t) \end{bmatrix} \tag{5.1}$$

where l_o, l_m are the near and far ends of the lossy section. $\boldsymbol{Y} \in \mathbb{R}^{2N\times 2N}$ is the Y-parameter matrix of the DEPACT cell

In order to apply wave form relaxation algorithm to the equation in (5.1), the Y-parameters matrix should be re-arranged using a permutation matrix to group the Y-parameters of each individual line together as follows [4]

$$\begin{bmatrix} i_1(l_0,t) \\ i_1(l_m,t) \\ i_2(l_0,t) \\ i_2(l_m,t) \\ \vdots \\ i_N(l_0,t) \\ i_N(l_m,t) \end{bmatrix} = \begin{bmatrix} Y_{11} & Y_{12} & \dots & Y_{1N} \\ Y_{21} & Y_{22} & \dots & Y_{2N} \\ \vdots & \vdots & \ddots & \vdots \\ Y_{N1} & Y_{N2} & \dots & Y_{NN} \end{bmatrix} \begin{bmatrix} v_1(l_0,t) \\ v_1(l_m,t) \\ v_2(l_0,t) \\ v_2(l_m,t) \\ \vdots \\ v_N(0,t) \\ v_N(l_m,t) \end{bmatrix} \tag{5.2}$$

where $Y_{jj} \in \mathbb{R}^{2\times 2}$, $1 < j < N$ is the Y-parameters of j^{th} line and Y_{jk}, $1 < k < N$, is the coupling between line j and line k.

Decoupling (5.2) using waveform relaxation results in the following differential equations for the j^{th} line [4]

$$\begin{bmatrix} i_j^{(r+1)}(l_0,t) \\ i_j^{(r+1)}(l_m,t) \end{bmatrix} = Y_{jj} \begin{bmatrix} v_j^{(r+1)}(l_0,t) \\ v_j^{(r+1)}(l_m,t) \end{bmatrix} + \sum_{\substack{k=1 \\ k\neq j}}^{N} Y_{jk} \begin{bmatrix} v_k^{(r)}(l_0,t) \\ v_k^{(r)}(l_m,t) \end{bmatrix} \tag{5.3}$$

and the WR sources of the j^{th} line can be written as [4]

$$\begin{bmatrix} i_{src}^{(r)}(l_0,t) \\ i_{src}^{(r)}(l_m,t) \end{bmatrix}_{(j)} = \sum_{\substack{k=1 \\ k\neq j}}^{N} Y_{jk} \begin{bmatrix} v_k^{(r)}(l_0,t) \\ v_k^{(r)}(l_m,t) \end{bmatrix} \tag{5.4}$$

From (5.4), the WR sources can be represented as current sources at the terminals of the lossy part in the DEPACT cell as shown in Fig 5.1 [4], where the resistive

network is calculated as presented in [3, 9] (reviewed in chapter 2). It can be seen that the WR sources in (5.3) is directly calculated in time domain.

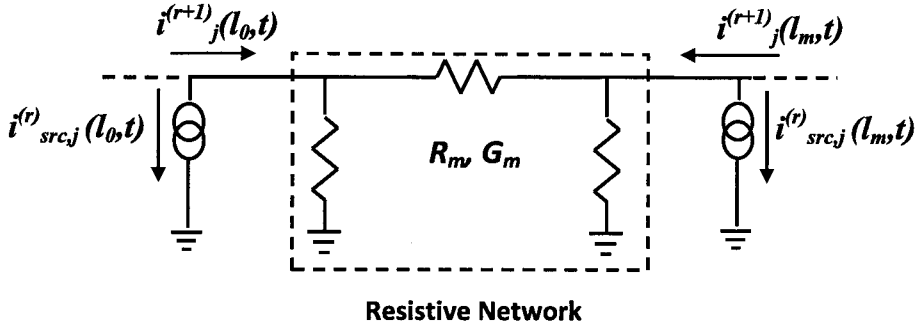

Figure 5.1: Equivalent circuit of the decoupled lossy section for the j^{th} line

5.2.2 Waveform Relaxation Sources of the Lossless Section

Consider a lossless section in the DEPACT macromodel. If $\tau_j = \sqrt{L_{jj}C_{jj}}$ is the delay of the line and $\boldsymbol{W_0}$ is the voltages / currents of the lossless sections of the N-lines at the near-end of each lossless section.

$$\boldsymbol{W}_0(t) = \begin{bmatrix} v_1(0,t) \\ v_2(0,t) \\ \vdots \\ v_N(0,t) \\ i_1(0,t) \\ i_2(0,t) \\ \vdots \\ i_N(0,t) \end{bmatrix} \tag{5.5}$$

It was shown in [4] that the WR sources of the lossless part for the j^{th} line can be given in a closed form as follows

$$\begin{bmatrix} \eta_j^{(r)}(\hat{l}_m,t) \\ \gamma_j^{(r)}(\hat{l}_m,t) \end{bmatrix} = -\boldsymbol{\beta}_j \begin{bmatrix} f_{j1}^{(r)}(t) \\ f_{j2}^{(r)}(t) \end{bmatrix} \tag{5.6}$$

where $f_{j1}(t)$ and $f_{j2}(t)$ are defined as

$$f_{j1}^{(r)}(t) = \sum_{p=1}^{N} \frac{\boldsymbol{K}_j^{(1,p)}}{\gamma_p - \tau_j} \left[\phi_p^{(r)}(t+\gamma_p\hat{l}_m)u(t+\gamma_p\hat{l}_m) - \phi_p^{(r)}(t+\tau_j\hat{l}_m)u(t+t_j\hat{l}_m)\right] \tag{5.7}$$

$$+ \sum_{p=N+1}^{2N} \frac{\boldsymbol{K}_j^{(1,p)}}{\gamma_{p-N} - \tau_j} \left[\phi_p^{(r)}(t+\gamma_{p-N}\hat{l}_m)u(t+\gamma_{p-N}\hat{l}_m) - \phi_p^{(r)}(t+\tau_j\hat{l}_m)u(t+t_j\hat{l}_m)\right] \tag{5.8}$$

$$f_{j2}^{(r)}(t) = \sum_{p=1}^{N} \frac{-\boldsymbol{K}_j^{(2,p)}}{-\gamma_p - \tau_j} \left[\phi_p^{(r)}(t+\gamma_p \hat{l}_m)u(t+\gamma_p \hat{l}_m) - \phi_p^{(r)}(t-\tau_j d_m)u(t-t_j d_m)\right] \quad (5.9)$$

$$+ \sum_{p=N+1}^{2N} \frac{-\boldsymbol{K}_j^{(1,p)}}{\gamma_{p-N} - \tau_j} \left[\phi_p^{(r)}(t-\gamma_{p-N} \hat{l}_m)u(t-\gamma_{p-N} \hat{l}_m) - \phi_p^{(r)}(t-\tau_j d_m)u(t-t_j \hat{l}_m)\right] \quad (5.10)$$

and

$$\begin{bmatrix} \phi_1^{(r)}(t) \\ \vdots \\ \phi_{2N}^{(r)}(t) \end{bmatrix} = \boldsymbol{\Gamma}^{-1} \boldsymbol{W}_0^{(r)}(t) \qquad \begin{bmatrix} 0 & -\boldsymbol{L} \\ -\boldsymbol{C} & 0 \end{bmatrix} = \boldsymbol{\Gamma} \;\; diag([\gamma_1, \ldots \gamma_N]) \;\; \boldsymbol{\Gamma}^{-1}$$

$$\boldsymbol{\beta}_j = eigenvectors\left(\begin{bmatrix} 0 & -L_{jj} \\ -C_{jj} & 0 \end{bmatrix}\right) \quad (5.11)$$

and $u(t)$ is the unit step function.

Due to the fact that we are dealing with a purely lossless line, the WR sources can be calculated in a closed form using (5.6), as a combination of delayed time domain waveforms of the voltages and currents at the near end of the lossless section [4]. Fig. 5.2 shows the equivalent circuit of a lossless DEPACT section with WR sources.

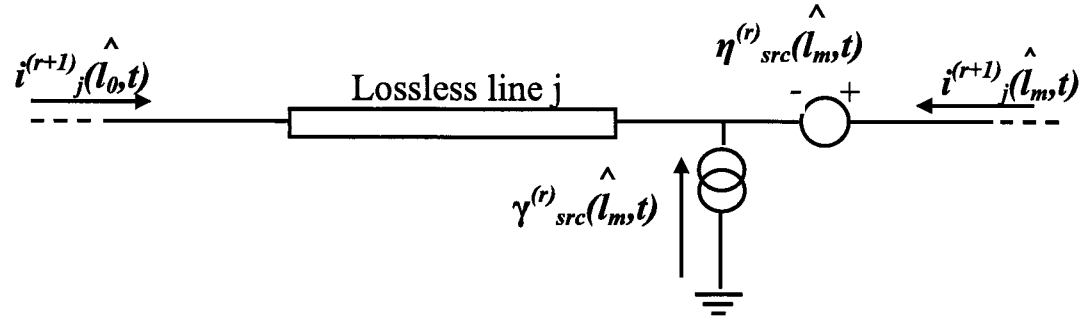

Figure 5.2: Equivalent circuit of the decoupled lossless section for the j^{th} line [4]

5.3 The Decoupling Strategy for the DEPACT Macromodel

Since the DEPACT macromodel consists of a lossy and lossless sections, WR sources are required for each cell. Therefore, increasing the number of sections results in a large number of WR sources attached to each line. This large number of sources limits the efficiency of MOR algorithm if applied directly to each partitioned line. To address this issue, Thevenin equivalent sources will be calculated to replace the WR sources for each line.

Since, the DEPACT macromodel contains delay elements, the MNA equations of the j^{th} line at the $(r+1)$ iteration can be written using (3.31) as follows [14]

$$\tilde{\boldsymbol{G}}_j^{(r+1)}\tilde{\boldsymbol{x}}_j^{(r+1)}(t)+\tilde{\boldsymbol{C}}_j\dot{\tilde{\boldsymbol{x}}}_j^{(r+1)}(t)=\sum_{k=1}^{2m}\tilde{\boldsymbol{A}}_k\tilde{\boldsymbol{x}}_j^{(r+1)}(t-\tau_k)+\tilde{\boldsymbol{B}}_j\boldsymbol{u}_{in}(t)+\boldsymbol{D}_j\begin{bmatrix}\boldsymbol{\eta}_j^{(r)}(t)\\ \boldsymbol{\gamma}_j^{(r)}(t)\\ \boldsymbol{i}_{src,j}^{(r)}(t)\end{bmatrix} \tag{5.12}$$

where

- m is the number of the DEPACT sections,
- $\tilde{\boldsymbol{G}}_j$, $\tilde{\boldsymbol{C}}_j$ are the same as (3.31),
- $\tilde{\boldsymbol{x}}_j$, $\tilde{\boldsymbol{B}}_j$ are the same as (3.32),
- $\boldsymbol{D}_j$ is a selector matrix,
- $\boldsymbol{\eta}_j \in \mathbb{R}^{2m}$, $\boldsymbol{\gamma}_j \in \mathbb{R}^{2m}$ are vectors that contain the values of the relaxation sources related to the lossless lines of the DEPACT sections,
- $\boldsymbol{i}_{src,j} \in \mathbb{R}^{2m}$ is a vector that contains the values of the relaxation sources related to the lossy lines of the DEPACT sections.

Since the WR sources are distributed throughout the line, Thevenin voltage sources are used to replace the WR sources at the two terminals of each line, as shown in Fig. 5.3. The Thevenin sources are evaluated by simulating the decoupled j^{th} line with open circuit at the terminations, Fig. 5.4. Using the equivalent Thevenin sources, (5.12) can be written as

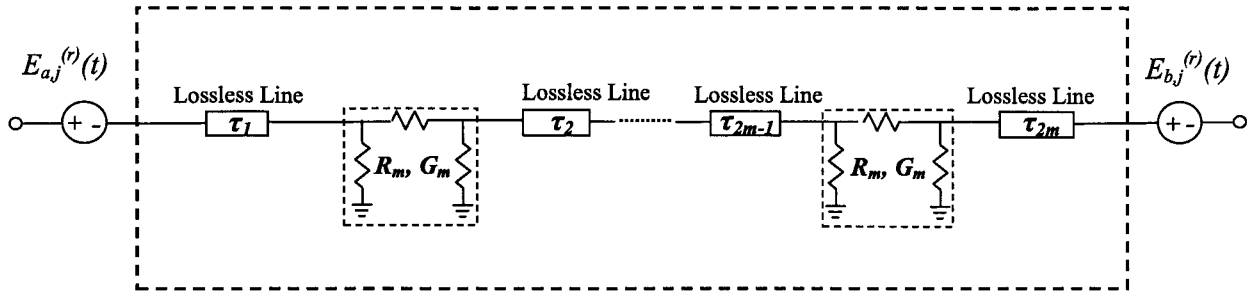

Figure 5.3: The equivalent circuit for the j^{th} line using Thevenin sources

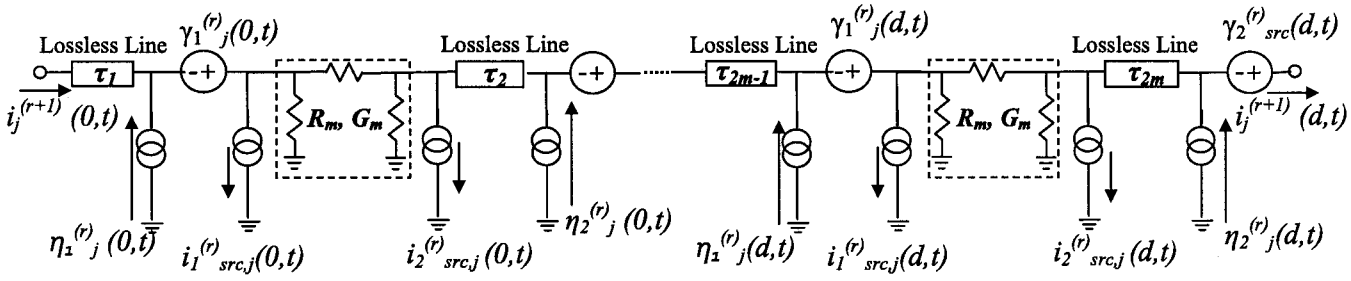

Figure 5.4: The j^{th} line with open circuit terminals to calculate Thevenin sources

$$\tilde{\boldsymbol{G}}_j\tilde{\boldsymbol{x}}_j^{(r+1)}(t)+\tilde{\boldsymbol{C}}_j\dot{\tilde{\boldsymbol{x}}}_j^{(r+1)}(t)=\sum_{k=1}^{2m}\tilde{\boldsymbol{A}}_{k,j}\tilde{\boldsymbol{x}}_j^{(r+1)}(t-\tau_k)+\tilde{\boldsymbol{B}}_j\boldsymbol{u}_{in,j}(t)+\boldsymbol{F}_j\begin{bmatrix}E_{a,j}^{(r)}(t)\\E_{b,j}^{(r)}(t)\end{bmatrix} \tag{5.13}$$

5.4 Reduction of the Decoupled Lines

Due to the presence of delay elements in the DEPACT macromodel, MOR algorithms such as PRIMA can not be directly applied to (5.13). Using the algorithm described

in [14] (reviewed in section 3.4), the network described by (5.13) can be reduced. The reduced MNA equations can be written as

$$\begin{aligned} \hat{\boldsymbol{G}}_j \hat{\boldsymbol{x}}_j^{(r+1)}(t) + \hat{\boldsymbol{C}}_j \hat{\dot{\boldsymbol{x}}}_j^{(r+1)}(t) &= \sum_{k=1}^{2m} \hat{\boldsymbol{A}}_{k,j}^{(r+1)} \hat{\boldsymbol{x}}_j^{(r+1)}(t - \tau_k) + \hat{\boldsymbol{B}}_j \boldsymbol{u}_{in,j}(t) \\ &+ \boldsymbol{Q}^T \boldsymbol{F}_j \begin{bmatrix} E_{a,j}^{(r)}(t) \\ E_{b,j}^{(r)}(t) \end{bmatrix} \qquad (5.14) \\ \boldsymbol{i}_{out,j}^{(r+1)}(t) &= \hat{\boldsymbol{B}}^T \hat{\boldsymbol{x}}_j^{(r+1)}(t) \qquad (5.15) \end{aligned}$$

where $\hat{\boldsymbol{G}}_j = \boldsymbol{Q}_j^T \tilde{\boldsymbol{G}}_j \boldsymbol{Q}_j$, $\hat{\boldsymbol{C}}_j = \boldsymbol{Q}_j^T \tilde{\boldsymbol{C}}_j \boldsymbol{Q}_j$, $\hat{\boldsymbol{A}}_{k,j} = \boldsymbol{Q}_j^T \tilde{\boldsymbol{A}}_{k,j} \boldsymbol{Q}_j$ and $\hat{\boldsymbol{B}}_j = \boldsymbol{Q}_j^T \tilde{\boldsymbol{B}}_j$. The Algorithm to calculate the orthogonal bases for the network with delay elements can be found in [14].

The reduced Y-parameters matrix of the j^{th} line can be calculated as

$$\hat{\boldsymbol{Y}}_j(s) = \hat{\boldsymbol{B}}_j^T (s\hat{\boldsymbol{C}}_j + \tilde{\boldsymbol{G}}_j - \sum_{k=1}^{2m} \hat{\boldsymbol{A}}_{k,j} e^{-s\tau_k})^{-1} \hat{\boldsymbol{B}}_j \qquad (5.16)$$

As discussed in chapter 3, the reduced Y-parameters matrix of each line is inserted in the MNA equations of the overall circuit and simulated with the non-linear elements in the complete circuit.

5.5 Evaluating the WR Sources

The Thevenin representation, shown in Fig. 5.3, is valid only at the two ports of the subcircuit, and hence, the result of the reduced circuit simulation can not be directly used to update the WR sources (discussed in chapter (4)). The WR sources can be updated using a similar relation as in (4.17). Using the relation in (4.17), the WR sources for the lossy line can be calculated as

$$\begin{bmatrix} i^{(r)}_{src,j}(l_0,t) \\ i^{(r)}_{src,j}(l_m,t) \end{bmatrix} = \sum_{\substack{k=1 \\ k\neq j}}^{N} \tilde{Y}_{jk} \left(\boldsymbol{P}_1 \boldsymbol{Q} \hat{\boldsymbol{x}}^{(r)}_k(t) + \begin{bmatrix} v^{(r)}_{k,oc}(l_0,t) \\ v^{(r)}_{k,oc}(l_m,t) \end{bmatrix} \right) \tag{5.17}$$

where $\boldsymbol{P}_1 \in [0,1]$ is a selector matrix that selects the voltages $v_k(l_0,t)$ and $v_k(l_m,t)$ of the lossy cell on the k^{th} line for each DEPACT section, $\hat{\boldsymbol{x}}^{(r)}_k$ are the reduced states of the k^{th} line at the r^{th} iteration when simulated using the Thevenin equivalent sources, $\boldsymbol{x}^{(r)}_{oc,k}$ is a vector that contains the voltages and currents of the k^{th} line when simulated with open terminals to find the Thevenin equivalent sources of the WR sources.

In addition, the WR sources for the lossless line can be re-calculated as follows

$$\begin{bmatrix} \eta^{(r)}_j(d_m,t) \\ \gamma^{(r)}_j(d_m,t) \end{bmatrix} = -\boldsymbol{\beta}_j \begin{bmatrix} f^{(r)}_{j1}(t) \\ f^{(r)}_{j2}(t) \end{bmatrix} \tag{5.18}$$

where $\boldsymbol{\beta}_j$ represents the coupling parameters for line j and is given in (5.11), $f_{j1}(t)$

and $f_{j2}(t)$ are defined as

$$\begin{aligned} f_{j1}^{(r)}(t) &= \sum_{p=1}^{N} \frac{\boldsymbol{K}_j^{(1,p)}}{\gamma_p - \tau_j} \left[\phi_p^{(r)}(t+\gamma_p d_m)u(t+\gamma_p d_m) - \phi_p^{(r)}(t+\tau_j d_m)u(t+t_j d_m)\right] \\ &+ \sum_{p=N+1}^{2N} \frac{\boldsymbol{K}_j^{(1,p)}}{\gamma_{(p-N)} - \tau_j} \left[\phi_p^{(r)}(t+\gamma_{(p-N)} d_m)u(t+\gamma_{(p-N)} d_m) - \phi_p^{(r)}(t+\tau_j d_m)u(t+t_j d_m)\right] \end{aligned} \tag{5.19}$$

$$\begin{aligned} f_{j2}^{(r)}(t) &= \sum_{p=1}^{N} \frac{-\boldsymbol{K}_j^{(2,p)}}{-\gamma_p - \tau_j} \left[\phi_p^{(r)}(t+\gamma_p d_m)u(t+\gamma_p d_m) - \phi_p^{(r)}(t-\tau_j d_m)u(t-t_j d_m)\right] \\ &+ \sum_{p=N+1}^{2N} \frac{-\boldsymbol{K}_j^{(1,p)}}{\gamma_{p-N} - \tau_j} \left[\phi_p^{(r)}(t-\gamma_{p-N} d_m)u(t-\gamma_{p-N} d_m) - \phi_p^{(r)}(t-\tau_j d_m)u(t-t_j d_m)\right] \end{aligned} \tag{5.20}$$

$\tau_j = \sqrt{L_{jj}C_{jj}}$ is the delay of the line and

$$\begin{bmatrix} \phi_1^{(r)}(t) \\ \vdots \\ \phi_{2N}^{(r)}(t) \end{bmatrix} = \boldsymbol{\Gamma}^{-1}\boldsymbol{W}_0^{(r)}(t) \tag{5.21}$$

$$\boldsymbol{W}_0^{(r)}(t) = \left(P_2 \boldsymbol{Q} \hat{\boldsymbol{x}}_{\phi,k}^{(r)}(t) + \boldsymbol{W}_{0,oc}^{(r)}(t)\right) \tag{5.22}$$

where $\boldsymbol{W_{0,oc}}$ is the voltages / currents of the lossless sections of the N-lines at the near-end of the lossless section when the line has open circuit terminations and $\boldsymbol{P_2} \in [0,1]$ is a selector matrix that selects the voltages and currents of the lossless cells on the

k^{th} line for each DEPACT section, $\boldsymbol{x}_{oc,k}^{(r)} \in \mathbb{R}^{N_{\phi,k}}$ is a vector that contains the voltages and currents of the k^{th} line at the r^{th} iteration when simulated with open terminals to find the Thevenin equivalent sources of the WR sources and q is the number of matched block moments.

5.6 Numerical Examples

In this section, numerical examples are presented to show the accuracy and speed of the proposed method. The transient response of the proposed method is compared with the transient response obtained from Direct LU on the full coupled DEPACT macromodel and MOR applied to the full coupled DEPACT macromodel. The transient response of the proposed method is in excellent agreement. Moreover, the computational cost of the proposed method only grows linearly with the number of lines.

5.6.1 Example 1

In this example, we consider four coupled lines with linear terminations shown in Fig. 5.5. The length of each line is 5 cm. The RLGC parameters of the coupled lines

are

$$\boldsymbol{R} = \begin{bmatrix} 1.24 & 0 & 0 & 0 \\ 0 & 1.24 & 0 & 0 \\ 0 & 0 & 1.24 & 0 \\ 0 & 0 & 0 & 1.24 \end{bmatrix} \Omega/cm \quad \boldsymbol{L} = \begin{bmatrix} 7.361 & 0.965 & 0.241 & 0.107 \\ 0.965 & 7.361 & 0.965 & 0.241 \\ 0.241 & 0.965 & 7.361 & 0.965 \\ 0.107 & 0.241 & 0.965 & 7.361 \end{bmatrix} nH/cm$$

$$\boldsymbol{G} = \begin{bmatrix} 0.01 & 0 & 0 & 0 \\ 0 & 0.01 & 0 & 0 \\ 0 & 0 & 0.01 & 0 \\ 0 & 0 & 0 & 0.01 \end{bmatrix} Mho/cm \, \boldsymbol{C} = \begin{bmatrix} 1.29 & -0.19 & -0.012 & -0.002 \\ -0.19 & 1.29 & -0.19 & -0.01 \\ -0.012 & -0.19 & 1.29 & -0.19 \\ -0.002 & -0.01 & -0.19 & 1.29 \end{bmatrix} pF/cm$$

The circuit is excited with a trapezoidal pulse voltage source. The rise/fall time of the pulse is 0.5 ns and the pulse width is 5 ns. The circuit was simulated using the proposed method and the full coupled DEPACT marcromodel (using W-element in Hspice to represent the lossy sections). The order of the DEPACT macromodel is 10 (estimated using [3] with a relative error of 10%). The number of required block moments for a good approximation is 8. The transient response for the proposed method after 3-iterations as compared to the DEPACT macromodel is shown in Fig. 5.6 - 5.8. As seen, the results are in excellent agreement.

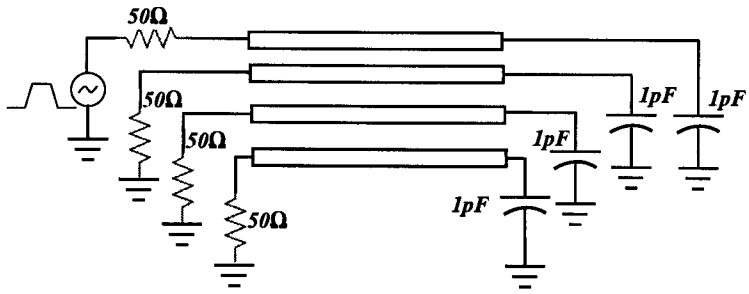

Figure 5.5: Four coupled lines with linear terminations (Example 1)

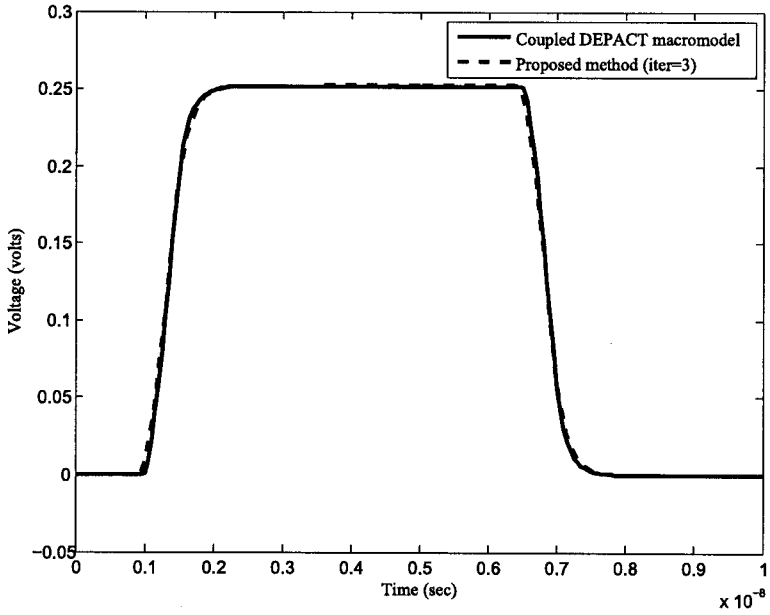

Figure 5.6: The transient response at far-end of line 1 (Example 1)

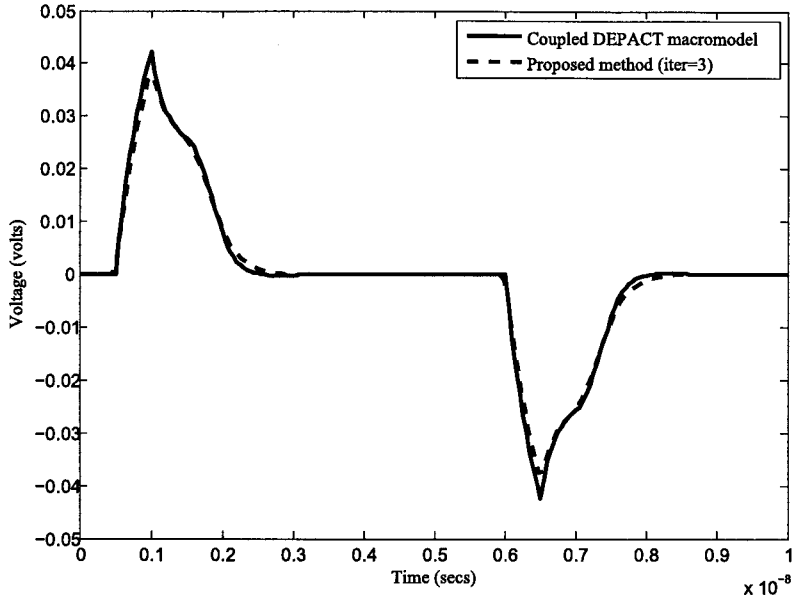

Figure 5.7: The transient response at near-end of line 2 (Example 1)

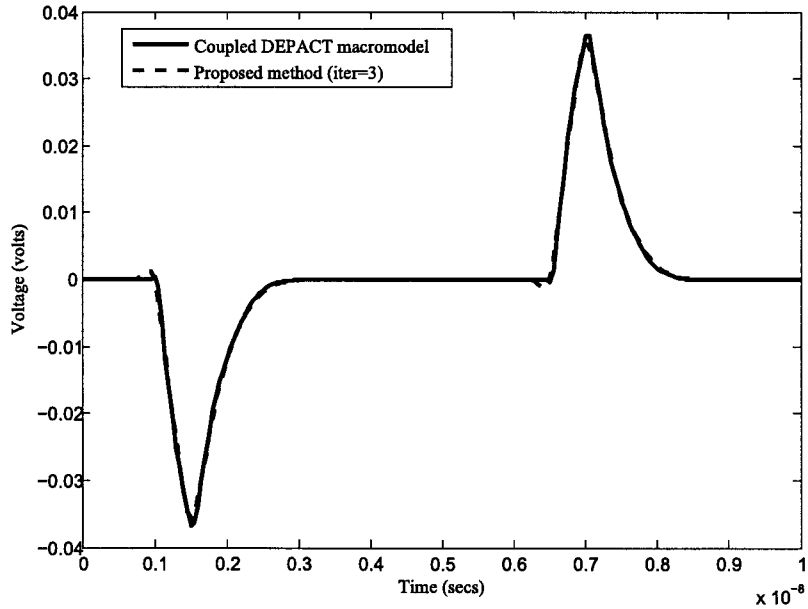

Figure 5.8: The transient response at far-end of line 2 (Example 1)

5.6.2 Example 2

In this example we consider the circuit shown in Fig. 5.9. The number of lines is varied from $30 < N < 60$. The circuit is excited with a trapezoidal pulse voltage source. The rise/fall time of the pulse is 0.1 ns and the pulse width is 5 ns. The length of each line is 10 cm. The number of DEPACT sections used is $m = 15$. Table 5.1 shows the CPU time to find the transient response of the full coupled TLs modeled as DEPACT, the response of MOR applied to the full coupled DEPACT macromodel, the transient response using the proposed method.

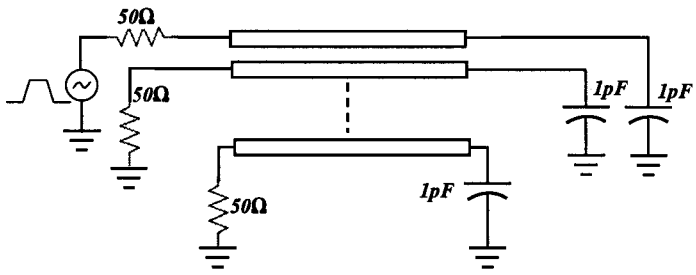

Figure 5.9: Interconnets circuit (Example 2)

Fig. 5.10 compares the CPU time to find the transient response of the full coupled TLs modeled as DEPACT, the time to find the response of MOR applied to the full coupled DEPACT macromodel, and the time to find the transient response of the proposed method. The proposed method grows linearly with the number of lines, in contrast to the coupled DEPACT macromodel and MOR when applied to the full DEPACT macromodel. It is to be noted that the size of the original MNA equations

for the 30 lines example is 1440 while the reduced model of the proposed method consists of 30 decoupled subcircuits each of size 20.

lines No.	Coupled TLs modeled as DEPACT (sec)	MOR applied to the coupled DEPACT (sec)	Proposed method (sec)
30	119.09	70.22	42.50
40	222.86	126.12	58.76
50	395.58	228.93	76.36
60	635.06	Out of Memory	92.76

Table 5.1: The CPU time comparison

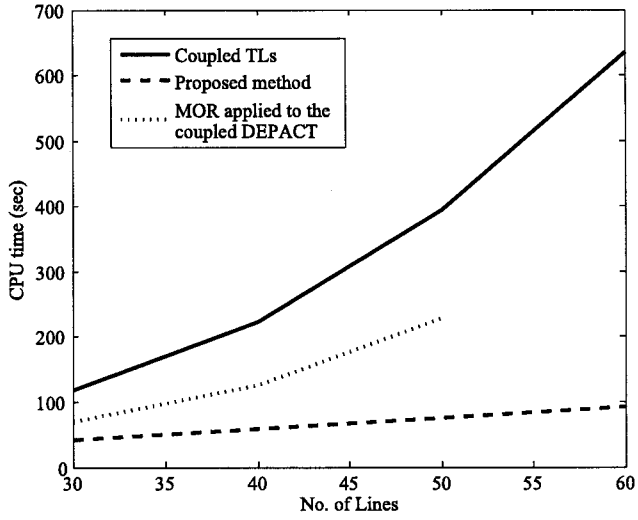

Figure 5.10: CPU time comparison

5.7 Summary

This chapter presented a new MOR method for massively coupled transmission lines modeled using DEPACT macromodel. Using waveform relaxation and transverse partitioning, the coupled transmission lines are separated into single line subcircuits. A MOR algorithm suitable for DEPACT macromodel is applied to each single line separately. Numerical examples were provided to validate the accuracy and the speed of the proposed method. The proposed method provides a very good accuracy. Moreover, the speedup only grows linearly with the number of lines.

Chapter 6

Conclusion and Future Research

6.1 Conclusion

One of the major limiting factors when applying model order reduction algorithms to interconnects circuits is the large number of ports. This limitation is related to the fact that the size of the reduced model increases dramatically with the increase in the number of ports.

In this thesis, an efficient passive model order reduction approach has been presented for massively coupled interconnect circuits [41]. This approach improves a recently proposed MOR method [12], which uses transverse partitioning and waveform relaxation to partition the coupled lines into independent single line subcircuit and model order reduction is then applied to each individual line separately. More-

over, an efficient transient simulation for the reduced model based on the generalized Thevenin theorem is presented.

In addition, a parallel simulation of the proposed approach has been presented. The simulation was done using the OpenMP library in C++. For each iteration, each individual line is simulated for the whole time duration in a separate processor. Once all lines are simulated, the WR-sources are updated and used to calculate the Thevenin sources for each line. It was shown that the speedup of the proposed method significantly increases with the increase in the number of processors.

The new MOR method [12] was extended to include the case of coupled transmission lines that are modeled with DEPACT sections. A reduction algorithm that is suitable for circuits with delay elements is used to reduce each independent line. Numerical examples were presented and the accuracy of the new method was compared to the Direct LU and conventional MOR methods. The CPU-time of the proposed method grows linearly with the number of lines.

6.2 Future Research

- The parallel implementation presented in this thesis (given in chapter 4) is only based on the physical transverse partitioning between the lines. However, a time-domain partitioning algorithm of the simulation task can be implemented. The time domain partitioning algo-

rithm was proposed in [45] as an efficient parallel algorithm of coupled transmission lines. However, it can be extended to include reduction of the lines using MOR. In the time partitioning algorithm [45], the simulation of each independent line is divided into several time blocks. Each time block is simulated separately, which allows more efficient scheduling among the available CPUs. Preliminary results show a very high improvement in the speedup characteristics when the time partitioning algorithm is used.

- The partitioned subcircuits used in the proposed algorithm contained single lines. However, in the case of two or more lines attached together to the same driver of receiver, the transverse partitioning will results in two or more lines subcircuits. Applying MOR to these subcircuits can be more efficient than simulating the original subcircuits in WR-TP algorithm.

- The MOR method that was previously proposed in [12] can be extended to include the case of frequency dependent (F.D) RLGC parameters. In the case of F.D parameters, a tabulated data from measurements or electromagnetic simulation is used to represent the F.D. RLGC parameters of the line. A vector fitting algorithm can be used

to fit the data with positive real rational functions followed by a passivity check algorithm to enforce the passivity of the resulting model.

References

[1] C. R. Paul, *Analysis of Multiconductor Transmission Lines.* New York: Wiley, 1994.

[2] R. Achar and M. Nakhla, "Simulation of high-speed interconnects," *Proceedings of the IEEE*, vol. 89, pp. 693–728, May 2001.

[3] N. M. Nakhla, "Analytical algorithms for macromodeling and senstivity analysis of high-speed interconnects," Master's thesis, Ottawa-Carleton institute for Electrical and Computer Engineering, 2005.

[4] N. M. Nakhla, "Waveform relaxation and transverse partitioning algorithms for simulation of massively coupled interconnects," Ph.D. dissertation, Ottawa-Carleton institute for Electrical and Computer Engineering, Nov. 2008.

[5] J. Branin, F.H., "Transient analysis of lossless transmission lines," *Proceedings of the IEEE*, vol. 55, pp. 2012 – 2013, Nov. 1967.

[6] S. G. Talocia, H. Huang, A. Ruehli, F. Canavero, and I. Elfadel, "Transient analysis of lossy transmission lines: an efficient approach based on the method of characteristics," *IEEE Transactions on Advanced Packaging*, vol. 27, pp. 45 – 56, Feb. 2004.

[7] A. Dounavis, X. Li, M. Nakhla, and R. Achar, "Passive closed-form transmission-line model for general-purpose circuit simulators," *IEEE Transactions on Microwave Theory and Techniques*, vol. 47, pp. 2450 – 2459, Dec. 1999.

[8] A. Dounavis, R. Achar, and M. Nakhla, "Efficient passive circuit models for distributed networks with frequency-dependent parameters," *IEEE Transactions on Advanced Packaging*, vol. 23, pp. 382 –392, Aug 2000.

[9] N. Nakhla, A. Dounavis, R. Achar, and M. Nakhla, "DEPACT: delay extraction-based passive compact transmission-line macromodeling algorithm," *IEEE Transactions on Advanced Packaging*, vol. 28, pp. 13–23, Feb. 2005.

[10] B. Moore, "Principal component analysis in linear systems: Controllability, observability, and model reduction," *IEEE Transactions on Automatic Control*, vol. 26, pp. 17–32, 1981.

[11] A. Odabasioglu, M. Celik, and L. T. Pileggi, "PRIMA: Passive reduced-order interconnect macromodeling algorithm," *IEEE Journal on Technology in Computer Aided Design*, pp. 645–654, Aug 1998.

[12] N. Nakhla, M. Nakhla, and R. Achar, "Sparse and passive reduction of massively coupled large multiport interconnects," in *IEEE/ACM International Conference on Computer-Aided Design, ICCAD*, Nov. 2007, pp. 622–626.

[13] N. Nakhla, A. Ruehli, M. Nakhla, and R. Achar, "Simulation of coupled interconnects using waveform relaxation and transverse partitioning," *IEEE Transactions on Advanced Packaging*, vol. 29, pp. 78–87, Feb. 2004.

[14] W. Tseng, C. Chen, E.Gad, M.Nakhla, and R.Achar, "Passive order reduction for RLC circuits with delay elements," *IEEE Transactions on Advanced Packaging*, vol. 30, pp. 830 –840, Nov. 2007.

[15] Q.-W. Xu, Z.-F. Li, J. Wang, and J.-F. Mao, "Transient analysis of lossy interconnects by modified method of characteristics," *IEEE Transactions on Circuits and Systems—Part I: Fundamental Theory and Applications*, vol. 47, pp. 363 –375, Mar. 2000.

[16] A. Dounavis, R. Achar, and M. Nakhla, "Addressing transient errors in passive macromodels of distributed transmission-line networks," *IEEE Trans-*

actions on Microwave Theory and Techniques, vol. 50, pp. 2759 – 2768, Dec. 2002.

[17] A. Dounavis, "Passive time-domain macromodels of high speed interconnect networks," Ph.D. dissertation, Carleton University, Dec. 2003.

[18] A. Dounavis, R. Achar, and M. Nakhla, "A general class of passive macromodels for lossy multiconductor transmission lines," *IEEE Transactions on Microwave Theory and Techniques*, vol. 49, pp. 1686–1696, Oct. 2001.

[19] N. Nakhla, M. Nakhla, and R. Achar, "Simplified delay extraction-based passive transmission line macromodeling algorithm," *IEEE Transactions on Advanced Packaging*, vol. 33, pp. 498–509, Oct. 2009.

[20] F. Chang, "Transient analysis of lossless coupled transmission lines in a nonhomogeneous dielectric medium," *IEEE Transactions on Microwave Theory and Techniques*, vol. 18, pp. 616 – 626, Sep. 1970.

[21] B. R., *Graduate Texts in Mathemetics.* New York: Springer, 1997.

[22] V.Raghavan, J. Bracken, and R.A.Rohrer, "AWESpice: a general tool for the accurate and efficient simulation of interconnect problems," in *Proceedings of Design Automation Conference, 29th ACM/IEEE*, June 1992, pp. 87 –92.

[23] R.Achar, M. P.K.Gunupudi, and E.Chiprout, "Passive interconnect reduction algorithm for distributed/measured networks," *IEEE Transactions on Circuits and Systems—Part II: Analog and Digital Signal Processing*, vol. 47, pp. 287 –301, Apr. 2000.

[24] M.Celik, L.Pileggi, and A.Odabasioglu, *IC Interconnect Analysis.* Philadelphia: Springer US, 2002.

[25] J. Vlach and K. Singhal, *Computer Methods for Circuit Analysis and Design.* New York: Van Nostrand, 1983.

[26] L.T.Pillage and R.A.Rohrer, "Asymptotic waveform evaluation for timing analysis," *IEEE Transactions on Computer-Aided Design of Integrated Circuits and Systems*, vol. 9, pp. 352 –366, Apr. 1990.

[27] R.Feldmann and R.W.Freund, "Efficient linear circuit analysis by Pade approximation via the Lanczos process," *IEEE Transactions on Computer-Aided Design of Integrated Circuits and Systems*, vol. 14, pp. 639 –649, May 1995.

[28] J. Demmel, *Applied Numerical Linear Algebra.* Philadelphia: SIAM, 1997.

[29] I.M.Elfadel and D. Ling, "A block rational arnoldi algorithm for multipoint passive model-order reduction of multiport RLC networks," *Proceedings of*

International Conference on Computer Aided Design (ICCAD), pp. 66–71, Nov. 1997.

[30] E. Gad and M. Nakhla, "An efficient algorithm for sensitivity analysis of nonuniform transmission lines," *IEEE Transactions on Advanced Packaging*, vol. 28, pp. 197 – 208, May. 2005.

[31] A. Ruehli and T. Johnson, *Circuit Analysis Computing by Waveform Relaxation, in Encyclopedia of Electrical and Electronics Engineering.* New York: John Webster, Wiley, 1999.

[32] E. Lelarasmee, A. Ruehli, and A. Sangiovanni-Vincentelli, "The waveform relaxation method for time-domain analysis of large scale integrated circuits," *IEEE Transactions on Computer-Aided Design of Integrated Circuits and Systems*, vol. 1, pp. 131 – 145, July 1982.

[33] J. White and A. Sangiovanni, "Relax2: A modified waveform relaxation approach to the simulation of cmos digital logic," in *IEEE international Symposium on Circuit and Systems*, May 1982.

[34] U. Miekkala and O. Nevanlinna, "Convergence of waveform relaxation method," in *IEEE International Symposium on Circuits and Systems*, vol. 2, June 1988, pp. 1643 – 1646.

[35] J. White and A. Sangiovanni-Vincentelli, *Relaxation Technique for the Simulation of VLSI Circuits.* Norwel, MA: Kluwer, 1987.

[36] E. Lelarasmee, "The waveform relaxation method for time domain analysis of large scale integrated circuits," Ph.D. dissertation, University of California, Berkeley; also Memo UCB/ERL M82/40, 1982.

[37] F. Y. Chang, "The generalized method of characteristics for waveform relaxation analysis of lossy coupled transmission lines," *IEEE Transactions on Microwave Theory and Techniques*, vol. 37, pp. 2028 –2038, Dec. 1989.

[38] R. Wang and O. Wing, "Transient analysis of dispersive VLSI interconnects terminated in nonlinear loads," *IEEE Transactions on Computer-Aided Design of Integrated Circuits and Systems*, vol. 11, pp. 1258 –1277, Oct. 1992.

[39] F. Y. Chang, "Waveform relaxation analysis of RLCG transmission lines," *IEEE Transactions on Circuits and Systems*, vol. 37, pp. 1394 –1415, Nov. 1990.

[40] N. Nakhla, A. Ruehli, M. Nakhla, R. Achar, and C. Changzhong, "Waveform relaxation techniques for simulation of coupled interconnects with frequency-dependent parameters," *IEEE Transactions on Advanced Packaging*, vol. 30, pp. 257 –269, May 2007.

[41] N. Nakhla, M. Farhan, A. Narayanan, M. Nakhla, and R. Achar, "Efficient model-order reduction of massively coupled multiport interconnects using waveform relaxation," *IEEE Transactions on Computer-Aided Design of Integrated Circuits and Systems*, submitted for publication.

[42] F. M. Tesche, M. V. Ivanov, and T. Karlsson, *EMC Analysis Methods and Computational Models.* New York: Wiley, 1997.

[43] T. A. Davis, *Direct Methods for Sparse Linear Systems.* Philadelphia: SIAM, 2006.

[44] A. Ruehli, A. Cangellaris, and H.-M. Huang, "Three test problems for the comparison of lossy transmission line algorithms," in *Proceedings of IEEE 11th Topical Meeting on Electrical Performance of Electronic Packaging*, Monterey, California, Oct. 2002, pp. 347–350.

[45] D. Paul, N. Nakhla, R. Achar, and M. Nakhla, "Parallel simulation of massively coupled interconnect networks," *IEEE Transactions on Advanced Packaging*, vol. 33, pp. 115 –127, Feb. 2010.